

University of Southern Queensland
Faculty of Engineering & Surveying

**Improving the Aerodynamic Force Measurement System
for the USQ Gun Tunnel**

A dissertation submitted by

Timothy Davidson

in fulfilment of the requirements of

ENG4112 Research Project

towards the degree of

Bachelor of (Engineering, Mechanical)

Submitted: October, 2004

Abstract

The accurate landing of entry capsules on other planets and moons depends on accurate knowledge of the aerodynamic behavior of the landing vehicle. The problem is that at the hypersonic speeds that are experienced by entry capsules during atmospheric entry, it is very hard to predict the capsule's behavior.

This project, *The Measurement of Entry Capsule Aerodynamic Force Coefficient* aims to improve the original aerodynamic force measurement system that is used in the University of Southern Queensland Gun Tunnel.

After an analysis of the previous method of force measurement and a review of other force measurement systems a new system was designed for the Gun Tunnel. This will allow for the prediction of normal and axial forces on an entry capsule model, as well as the location of the centre of pressure.

The first test run of this project aimed to identify the aerodynamic forces acting on the Japanese, MUSES-C Entry Capsule during a Mach 7 flow in the USQ Gun Tunnel. During this test only the axial force was measured. This force was then compared to a prediction based on a Newtonian Flow model.

University of Southern Queensland
Faculty of Engineering and Surveying

ENG4111/2 <i>Research Project</i>
--

Limitations of Use

The Council of the University of Southern Queensland, its Faculty of Engineering and Surveying, and the staff of the University of Southern Queensland, do not accept any responsibility for the truth, accuracy or completeness of material contained within or associated with this dissertation.

Persons using all or any part of this material do so at their own risk, and not at the risk of the Council of the University of Southern Queensland, its Faculty of Engineering and Surveying or the staff of the University of Southern Queensland.

This dissertation reports an educational exercise and has no purpose or validity beyond this exercise. The sole purpose of the course pair entitled “Research Project” is to contribute to the overall education within the student’s chosen degree program. This document, the associated hardware, software, drawings, and other material set out in the associated appendices should not be used for any other purpose: if they are so used, it is entirely at the risk of the user.

Prof G Baker

Dean

Faculty of Engineering and Surveying

Certification of Dissertation

I certify that the ideas, designs and experimental work, results, analyses and conclusions set out in this dissertation are entirely my own effort, except where otherwise indicated and acknowledged.

I further certify that the work is original and has not been previously submitted for assessment in any other course or institution, except where specifically stated.

TIMOTHY DAVIDSON

001122275

Signature

Date

Acknowledgments

Thanks to Dr David Buttsworth for providing this topic and the guidance and time that he gave. I would also like to thank Dr Ahmed Sharifian for his input and all of my family and friends for their patience and continued support.

TIMOTHY DAVIDSON

University of Southern Queensland

October 2004

Contents

Abstract	i
Acknowledgments	iv
List of Figures	xi
List of Tables	xiv
Nomenclature	xv
Chapter 1 Introduction	1
1.1 Importance of Testing	1
1.1.1 Muses-C Re-entry Capsule	2
1.2 Overview of the Dissertation	3
Chapter 2 Hypersonic Flow and Aerodynamic Forces	4
2.1 Chapter Overview	4
2.2 Flow Categories	5

CONTENTS	vi
2.2.1 Disturbance Effects	5
2.2.2 Hypersonic Flow	7
2.3 Predicting Forces caused by Hypersonic Flow	9
2.4 Chapter Summary	12
Chapter 3 Hypersonic Aerodynamic Force Measurement	13
3.1 Chapter Overview	13
3.2 Types of Testing Facilities	14
3.2.1 Shock Tubes	14
3.2.2 Arc-heated Test Facilities	15
3.2.3 Ballistic Free Flight Ranges	15
3.2.4 Hypersonic Wind Tunnels	16
3.3 The USQ Gun Tunnel	16
3.3.1 Facility Layout	16
3.3.2 Gun Tunnel Operation	17
3.4 Force Measurement Systems	19
3.4.1 Calibration	21
3.5 The USQ Force Measurement System	22
3.5.1 Measurement of Strain	23
3.6 Chapter Summary	25

Chapter 4	Analysis of Original System	26
4.1	Chapter Overview	26
4.2	Original Results	26
4.2.1	Expected Results	28
4.3	Bench testing of original system	28
4.3.1	Method	28
4.3.2	Summary of Results	30
4.4	Use of Piezoelectric Strain Gauges	31
4.4.1	Material Properties	32
4.4.2	Problems with Piezoelectric Strain Gauges	33
4.5	Required Areas of Improvement	33
4.6	Chapter Summary	35
Chapter 5	Improvement of the existing System	36
5.1	Chapter Overview	36
5.2	Method of Improvement	36
5.2.1	Improving the Frequency Response	36
5.2.2	Improving the Damping Properties	39
5.2.3	Improving the Piezoelectric Output	40
5.2.4	Accurately Determining the Centre of Pressure	41
5.3	Design of the New System	42

5.3.1	Frequency Prediction	43
5.3.2	Piezoelectric Accuracy	44
5.4	Bench Testing the New System	46
5.4.1	Initial Calibration of Piezoelectric Films	46
5.4.2	Expected Piezoelectric Output	47
5.4.3	Frequency Response	48
5.5	Chapter Summary	50
Chapter 6 Test Run Setup		51
6.1	Chapter Overview	51
6.2	Measurement Setup	52
6.2.1	Oscilloscope	52
6.2.2	Charge amplifier	53
6.3	Connection of piezoelectric films	53
6.3.1	Protection from Flow Effects	54
6.4	Problems	54
6.5	Chapter Summary	56
Chapter 7 Results and Discussion		57
7.1	Chapter Overview	57
7.2	Flow Quality	57

7.3	Measured Results	58
7.3.1	Piezoelectric Response	60
7.4	Finding the Aerodynamic Force	61
7.4.1	Calibration	61
7.4.2	Force Calculation	63
7.5	Expected Results	64
7.5.1	Sources of Error	64
7.6	Chapter Summary	67
Chapter 8 Conclusions and Further Work		68
8.1	Achievement of Project Objectives	68
8.2	Further Work	69
References		71
Appendix A Project Specification		73
Appendix B System Drawings		75
B.1	Original Drawings	76
B.2	Improved component	87
Appendix C Calculations		89
C.1	Force Prediction	90

CONTENTS

x

C.2 frequency prediction calculations	92
C.3 Calibration	95
C.4 Calculating the Aerodynamic Force from Measured Strains	97
Appendix D Source Code	100
D.1 Loadwavestar2	101
D.2 smo	102

List of Figures

2.1	Disturbance Effects	6
2.2	Particle motion in Newtonian Flow	8
2.3	Variation of stagnation pressure coefficient with M	10
2.4	Nomenclature for spherically blunted cones	11
3.1	Example of diaphragms	17
3.2	Diagram of Gun Tunnel layout	18
3.3	Single-component stress-wave force-balance	20
3.4	The existing mounting arrangement	22
3.5	System description	23
4.1	Results of the previous Force Measurement System	27
4.2	Rate of decay of oscillation measured by the logarithmic decrement	30
4.3	Cross section of piezoelectric strain gauge. (Smith p .7)	32
5.1	Graph showing the effect that changing the mass of the model has on the frequency of the system	37

5.2	Graph showing the effect that changing the length of the cantilever has on the frequency of the system.	38
5.3	Location of the centre of pressure	42
5.4	New system setup (with piezoelectric strain gauges)	43
5.5	Sketch of how the system will be modelled for natural frequency prediction	44
5.6	Graph used for calibration of piezoelectric films	47
5.7	The frequency response of the system	49
5.8	The frequency response of the system with tape connection	49
6.1	Location of BNC connection on test section wall	53
6.2	Wires protected from flow region	54
7.1	Graph showing average pressure during force measurement	58
7.2	Results of strain measurement system for the test run	59
7.3	Smooth results of test run	59
7.4	Graph of response of piezoelectric films to pressure changes	60
7.5	Example of calibration data	61
7.6	Graph used to determine sensitivity of first Piezo film	62
7.7	Graph used to determine sensitivity of second Piezo film	62
B.1	The new I-beam cantilever	88
C.1	Cross section of the I-Beam cantilever	93

C.2 Diagram of calibration setup 95

List of Tables

3.1	Performance parameters of the Gun Tunnel	19
4.1	Expected forces in high pressure Gun Tunnel test (at Mach 7)	28
4.2	Summary of Initial Bench Testing	31
5.1	Effect of alternative materials on the natural frequency	39
5.2	Important values for calibration of a piezoelectric strain gauge	47
7.1	Data from calibration of no. 1 Piezo film	63
7.2	Data from calibration of no. 2 Piezo film	63
7.3	Forces measured for Low pressure test run	63
7.4	Forces expected for low pressure test run	64

Nomenclature

A	Area (m^2)
c	Speed of sound in a medium ((m/s)
C_A	Axial force coefficient
C_N	Normal force coefficient
C_{pt2}	Stagnation point pressure coefficient
E	Modulus of Elasticity (Pa)
f	Frequency (Hz)
F	Force (N)
I	Moment of inertia (m^4)
l	Length (m)
M	Mach number; Moment(Nm)
m	Mass(kg)
P	Pressure (Pa)
Q	Charge output (Coulombs)
r	Cross-sectional radius
R_B	Base radius (m)
R_N	Nose radius (m)
t	Time (s)
U or V	Velocity (m/s)
α	Angle of attack
ε	Strain
ρ	Density (kg/m^3)
σ	Stress (Pa)

Subscripts

- 0 Stagnation conditions
- 1 or ∞ Free stream conditions
- 2 Properties immediately downstream of the shock wave

Chapter 1

Introduction

This project, *Improving the Aerodynamic Force Measurement System* aims to improve the existing aerodynamic force measurement system that is used in the University of Southern Queensland Gun Tunnel. The extension of the existing method will allow for the measurement of normal and axial forces on an entry capsule model, as well as the location of the centre of pressure.

The accurate landing of entry capsules on other planets and moons depends on accurate knowledge of the aerodynamic behavior of the landing vehicle. The problem is that at the hypersonic speeds that are experienced by entry capsules during atmospheric entry, it is very hard to predict their behavior. This means that to land within ten kilometers of an expected destination is a very good result.

As part of this project the aerodynamic forces on the MUSES-C re-entry capsule will be identified, through testing in the USQ Gun Tunnel. The results will be compared with analytical simulations of the vehicle performance.

1.1 Importance of Testing

As an aircraft or entry vehicle moves through the Earth's atmosphere it is subject to a number of forces caused by aerodynamic effects. Therefore, to successful design these

aircraft it is very important that imposed forces can be predicted so the behavior of the entry capsule when it approaches the earth can be understood.

This is where facilities such as the USQ Gun Tunnel are of use. The testing a scale models in controlled conditions is a cost effective way of simulating model behavior before and actual prototype is constructed.

In 2001, fourth year project student, Justin Terhorst, carried out work on the existing system. The model that he used for testing was the Japanese entry capsule, Muses-C. Therefore it would be sensible to use this model initially for testing.

1.1.1 Muses-C Re-entry Capsule

To give an indication of the applications of this project, the Muses-C re-entry mission will be described.

Muses-C is an asteroid return mission managed by the institute of Space and Astronautical Science (ISAS). Muses-C Was launched in December 2002 on an asteroid return mission which aims to travel 290 million kilometers, take a small sample and then return to the earth's surface. It is expected to return to Earth in 2007. In an application such as this, if the forces upon entry can be accurately predetermined, then the accuracy of the landing can be increased. It must be realised that as soon as the capsule separates from the main spacecraft it cannot be steered, therefore its aerodynamic performance must be accurately modelled . The re-entry of Muses-C will rely solely on aerodynamic stability for a controlled decent and has a landing footprint of 65km by 20km.

The re-entry capsule which is 40cm diameter \times 20cm deep an weighs 25kg and will enter the Earth's atmosphere at a velocity of over 12 km/s. This project will aim to measure the forces acting on a scale model of this re-entry capsule during hypersonic flight.

1.2 Overview of the Dissertation

This dissertation is organized as follows:

Chapter 2 gives a basic background on the importance of hypersonic flow and associated phenomena. This chapter emphasises the importance of aerodynamic forces in aircraft design and how the forces on a re-entry capsule can be estimated.

Chapter 3 presents a broad overview of how aerodynamic forces are measured at hypersonic speeds. This includes a description of different testing facilities and various force measurement systems. The USQ Gun Tunnel and force measurement system are also described in this.

Chapter 4 analyses the performance of the original USQ force measurement system. After reviewing the results of this system, the problem areas are identified.

Chapter 5 identifies ways of improving the force measurement system. In this chapter the improved system is developed and bench tested. The systems performance is also analysed.

Chapter 6 describes the setup of the first low pressure test run. This details the settings for the electrical equipment and highlights some of the problems that were experienced.

Chapter 7 contains all results from the test run combined with the calibration for this test. These results are analysed and are used to calculate the aerodynamic forces that are acting on the model. These forces are then compared to a theoretical prediction and conclusions are drawn about the accuracy of the system.

Chapter 8 concludes the dissertation and suggests further work that would be required to improve and validate the results that are obtained through measurements taken in the USQ Gun Tunnel.

Chapter 2

Hypersonic Flow and Aerodynamic Forces

2.1 Chapter Overview

As any body moves through a fluid it will be subject to a number of forces. The magnitude of these forces is dependent on a number of factors which include.

- Fluid Properties.
- Body shape and size, and importantly
- the relative speed of the body to the flow.

In the design of re-entry vehicles and high speed aircraft the identification of these forces experimentally and analytically is a critical part of the whole process. In the testing of these models it is essential to create a similar type of flow to what would be experienced during atmospheric entry.

This chapter will give a brief background on the theory behind hypersonic flow and how it is important in the testing of scale model re-entry capsules.

2.2 Flow Categories

As a body moving through a fluid increases in velocity, the effect it has on the surrounding air will change and the forces will increase dramatically, particularly as the body approaches the speed of sound, or Mach 1. The Mach number can be defined as the speed of the body relative to the speed of sound in a particular medium.

$$M = \frac{V}{c} \quad (2.1)$$

Generally flows can be described as *subsonic* where ($M < 1$) or *supersonic*, ($M > 1$). Flow fields that exhibit both subsonic and supersonic characteristics (usually between M 0.9 & M 1.2) can be termed *transonic* (Fox 1998, p. 599). The other flow regime that is of particular interest to this report is Hypersonic Flow, where the speed increases above Mach five ($M > 5$). It is important to distinguish between these flow regimes as the aerodynamic effect on an object varies greatly depending on the flow regime. For example, the aerodynamics at hypersonic speed are even different to those at supersonic speeds.

2.2.1 Disturbance Effects

The aerodynamic effects associated with subsonic and supersonic speeds are very different. This can be illustrated by comparing the effect of the moving body on the surrounding air in subsonic and supersonic flow.

It is known that any disturbance introduced at a point in a fluid will not immediately take effect through the entire medium. The disturbance will propagate through waves that move away from the origin. This speed is in no way related to the size of the disturbance and is actually the speed of sound in that medium. This can be seen in figure 2.1(a) This speed depends on the fluid properties such as temperature, pressure and density.

If the source of disturbance is moving, then the effect it has on the surrounding fluid

will vary depending on its velocity. If the source is moving at a velocity less than the speed of sound ($M < 1$), waves will still propagate away from the source in all directions at the speed of sound (as illustrated by figure 2.1(b)). As the speed of the source increases towards M1 these waves will become concentrated to a narrow region in front of the disturbance source (shown by figure 2.1(c)).

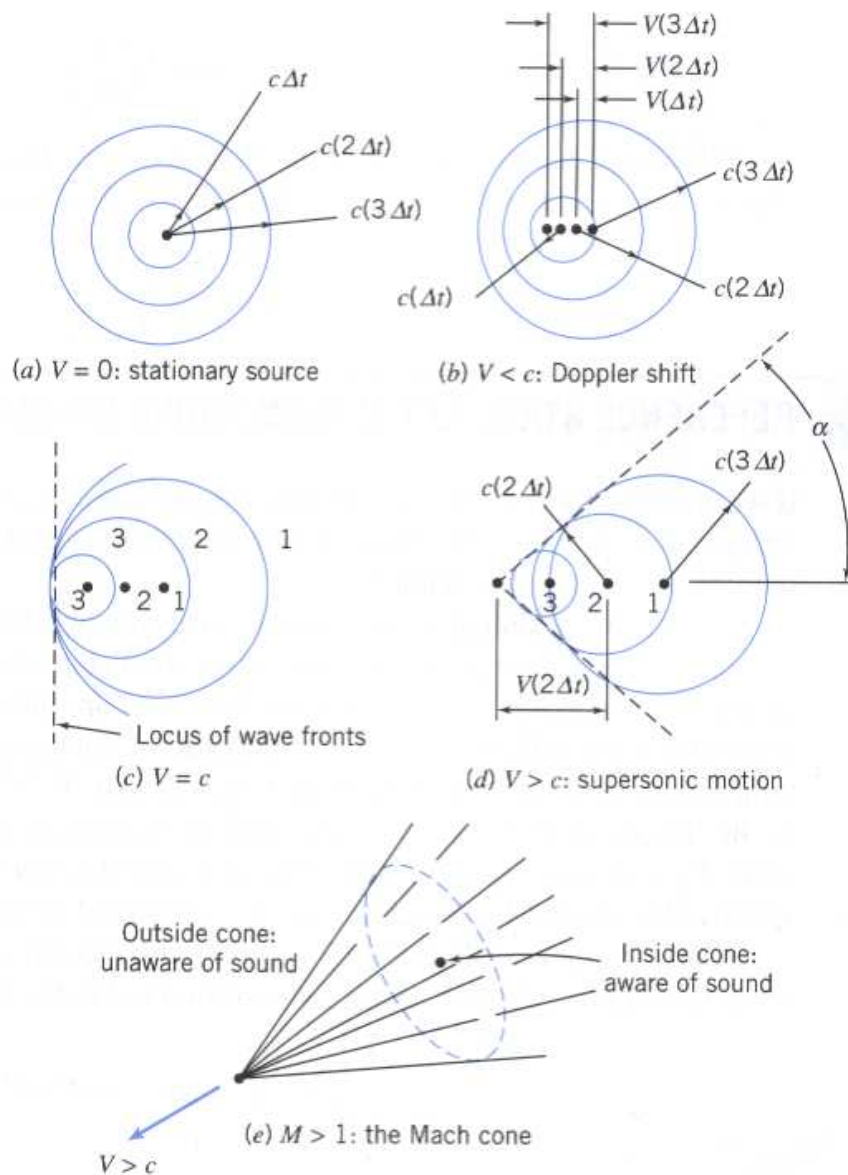


Figure 2.1: Disturbance Effects
(Duncan 1974, p. 159)

However, when the speed becomes greater than Mach 1, all of the spherical waves

produced by the disturbance are swept downstream of the source. If the flow is steady, the disturbance waves will lie within a circular cone (known as a *Mach Cone*) where the source is at the apex (figure 2.1(d)). Outside of this cone, the fluid will remain unaffected. The edges of the mach cone where the disturbance effect is concentrated are known as *Mach Waves*.

When the velocity of the disturbance is supersonic, it presents a front of very rapid, almost discontinuous compression to the oncoming fluid which is know as a *Shock Wave* (Duncan 1974). In crossing a 'shock' there is a rapid increase in pressure, a rapid rise in the density and temperature of the fluid and a fall in velocity. This one of the important phenomena associated with Supersonic and hypersonic flow. In fact, the process of change over a shock wave is so rapid and the thickness of the wave is so small that it is often treated as a discontinuity in the flow.

2.2.2 Hypersonic Flow

Hypersonic flow is defined as "the regime where certain flow phenomena become progressively more important as the Mach Number is increased to higher values" (John D. Anderson 1989, p. 13). Duncan (1974) describes Hypersonic flow as flow past a body at sufficiently high Mach numbers that is characterised by the fact that the leading edge shock waves lie close to the body surface. In some cases this can be as low as Mach 3, but as a rule of thumb is generally above Mach 5. Hypersonic flow is differentiated by the way that the flow pattern undergoes little change with an increase in Mach Number.

For a given flow deflection (or flow over a body), the density increase across the shock wave becomes progressively larger as the flow speed increases. At these higher densities, the mass flow behind the shock can more easily squeeze through a smaller area resulting in a small distance between the shock wave and the body. This flowfield between the shock wave and the hypersonic body is know as the *shock layer*. Some important characteristics associated with hypersonic flow are:

- The shock waves are close to the body, (therefore thin shock wave theory can be

used).

- Hypersonic flow creates high temperatures.
- There will be viscous interaction between the fluid and body.

In Hypersonic Theory, for flow over simple shapes, it can be assumed that the speed and direction of the gas particles in the freestream will remain unchanged until such time as they strike the solid that is exposed to the flow. This flow model is termed *Newtonian Flow*. In this flow model the normal component of the momentum of the approaching particle is cancelled out, whereas the tangential component of the momentum is conserved. This is illustrated by figure 2.2 where only the tangential component of the velocity ($U_{\infty, t}$) is conserved, not the normal component ($U_{\infty, n}$). Because energy cannot be destroyed, the kinetic energy that is lost by the particles through contact with the body is in turn released causing high temperatures at the contact surface.

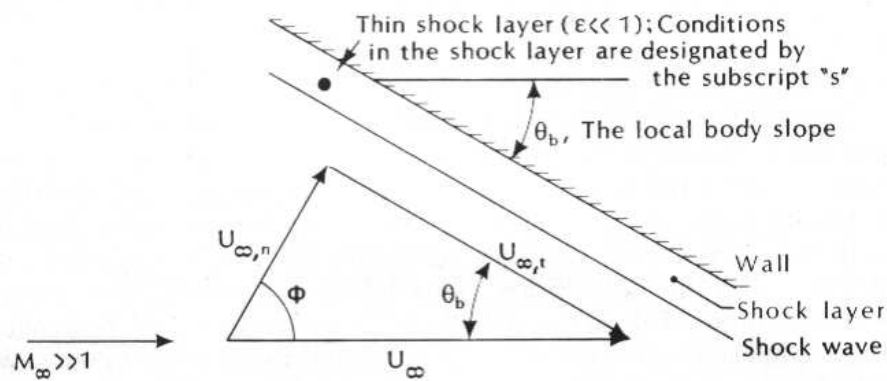


Figure 2.2: Particle motion in Newtonian Flow
(Bertin 1994, p. 6)

By using the momentum equation and the Newtonian flow model, the local pressure on the body can be determined in terms of the pressure coefficient.

Pressure coefficient (C_p) (Bertin 1994, p. 6)

$$C_p = \frac{p_w - p_{\infty}}{\frac{1}{2}\rho_{\infty}U_{\infty}^2} = 2 \sin^2 \theta_b = 2 \cos^2 \phi \quad (2.2)$$

Where number 2 represents the stagnation point pressure coefficient, C_{p2} , for Newtonian Flow (Bertin, p.6). (The stagnation point pressure coefficient relates to the pressure at the point on the body where the fluid has zero velocity). This pressure coefficient could then be used to calculate the normal and axial force coefficients. In these equations the local body slope (relative to the flow) is represented by θ_b

Alternatively the equation can be written (Bertin 1994, p .279)

$$C_p = C_{p2} \sin^2 \theta_b = C_{p2} \cos^2 \phi \quad (2.3)$$

This is termed *Modified Newtonian Flow*. For the modelling of flow over blunt bodies the modified newtonian equation (2.3) is considerably more accurate than the standard equation(2.2) .

The ability to test in hypersonic flow in the USQ Gun Tunnel is very important as the behaviour of the fluid in hypersonic flow is physically different from that in in subsonic and even supersonic flow. (This can be further illustrated by comparing hypersonic vehicles to subsonic aircraft.)

While the focus of this project is to actually measure aerodynamic forces in a controlled environment, it is also important that the forces on a particular body in hypersonic flow can be predicted whether this be analytically, or through computational methods.

2.3 Predicting Forces caused by Hypersonic Flow

There are various methods of predicting the forces that will act on a model during hypersonic flow. One analytical method that will be suitable for this application as mentioned previously is the modified Newtonian flow model.

In order to calculate the forces acting on the re-entry capsule the pressure distribution must be calculated using the stagnation point pressure coefficient C_{p2} (Bertin p.287),

$$C_{pt_2} = \left[\frac{p_{t_2}}{p_1} - 1 \right] \frac{2}{\gamma M_1^2} \quad (2.4)$$

Where the ratio of pressures $\frac{p_{t_2}}{p_1}$ can be found using (Bertin 1994, p. 288). This is the ratio of the pressure difference across the shock wave.

$$\frac{p_{t_2}}{p_1} = \left[\frac{(\gamma + 1)M_1^2}{2} \right]^{\frac{\gamma}{\gamma+1}} \left[\frac{\gamma + 1}{2\gamma M_1^2 - (\gamma - 1)} \right]^{\frac{1}{\gamma-1}} \quad (2.5)$$

This pressure coefficient can also be checked using the graph in figure 2.3.

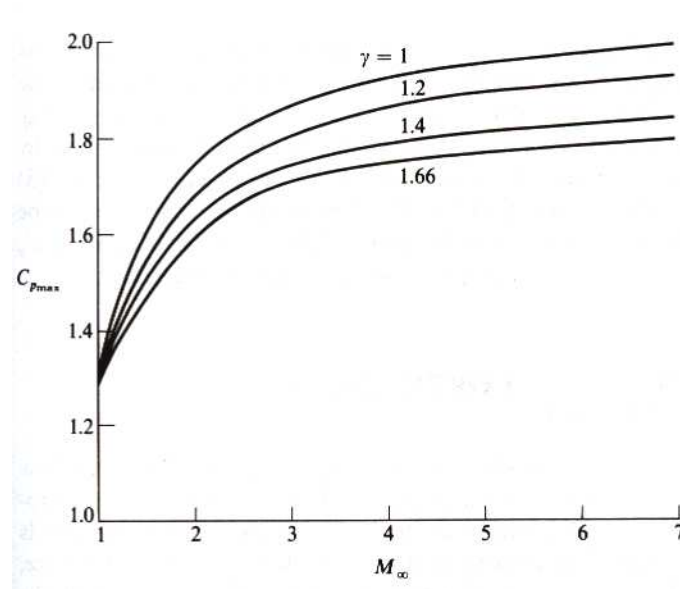


Figure 2.3: Variation of stagnation pressure coefficient with M (John D. Anderson 1989, p. 55)

The stagnation point pressure coefficient can then be used to determine the force coefficients (Bertin 1994, p. 468-470). The force coefficient equations (2.6 & 2.7) are dependent on the body shape and angle of attack. The nomenclature for these equations for blunt bodies (similar to MUSES-C) can be seen in figure 2.4.

Normal Force Coefficient:

$$C_N = 2C_{p,t2} \left(\frac{R_N}{R_B} \right)^2 \left[\begin{array}{l} 0.25 \sin \alpha \cos \alpha \cos^4 \theta_c + \sin \alpha \cos \alpha \sin \theta_c \cos \theta_c \times \\ \left(\frac{(R_B/R_N) - \cos \theta_c}{\tan \theta_c} \cos \theta_c + \frac{((R_B/R_N) - \cos \theta_c)^2}{2 \tan \theta_c} \right) \end{array} \right] \quad (2.6)$$

Axial Force Coefficient:

$$C_A = 2C_{p,t2} \left(\frac{R_N}{R_B} \right)^2 \left[\begin{array}{l} (0.25 \cos^2 \alpha (1 - \sin^4 \theta_c) + 0.125 \sin^2 \alpha \cos^4 \theta_c) + \\ \tan \theta_c (\cos^2 \alpha \sin^2 \theta_c + 0.50 \sin^2 \alpha \cos^2 \theta_c) \times \\ \left(\frac{(R_B/R_N) - \cos \theta_c}{\tan \theta_c} \cos \theta_c + \frac{((R_B/R_N) - \cos \theta_c)^2}{2 \tan \theta_c} \right) \end{array} \right] \quad (2.7)$$

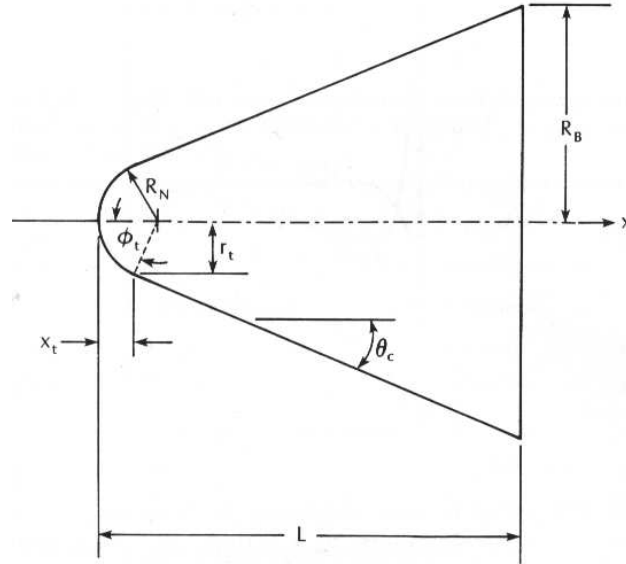


Figure 2.4: Nomenclature for spherically blunted cones
(Bertin 1994, p. 465)

Finally, by using the equations below the actual forces on the model can be predicted.

In this case, r is represented by R_B .

$$F_N = C_N \rho_1 U_1^2 \Pi r^2 \quad (2.8)$$

$$F_A = C_A \rho_1 U_1^2 \Pi r^2 \quad (2.9)$$

2.4 Chapter Summary

This chapter has given a brief overview of the phenomenon associated with the various flow regimes, in particular hypersonic flow.

It has also given an introduction to aerodynamic Forces and outlined how to estimate the aerodynamic forces acting on the a blunt body (such as the Muses-C spacecraft).

Chapter 3

Hypersonic Aerodynamic Force Measurement

3.1 Chapter Overview

In the design of aircraft it is important that the theoretical and computational predictions (that have already been discussed) can be combined with an experimental testing program.

Only real flight tests on a full scale model can create a completely accurate picture of vehicle behaviour. However it is obvious that these tests can only occur after extensive design, development, construction and therefore considerable cost. For this reason, the majority of of experimental information is obtained from ground based testing facilities.

Since complete simulations of a flowfield cannot be recorded at ground based facilities, it is important that the objectives of the tests are clearly outlined. Some common aims of testing include; (Bertin 1994)

1. Obtaining data to define the aerodynamic forces and moments or heat transfer distributions for configurations whose complex flowfields resist computational modeling .

2. Obtaining detailed data to be used in developing computational flow models (code validation).
3. Determine measurements of parameters, such as heat transfer and drag that can be compared to computed solutions.

Just as there are a numerous reasons for conducting hypersonic tests, there are a number of different types of testing facilities. This chapter will describe some of the major types of testing facilities and look at the different ways that aerodynamic forces are measured. It will also include a brief description of the USQ Gun Tunnel and the system that was employed to measure aerodynamic forces in hypersonic flows.

3.2 Types of Testing Facilities

There are a number of different types of testing facilities that can be used to replicate the aerothermodynamic environment of re-entry capsules. The type of facility, due to the differences in the flows created, can have a large bearing on how aerodynamic forces will be measured at that facility. Four main types of ground based hypersonic testing facilities are; Shock Tubes, Arc Heated test Facilities, Hypersonic wind tunnels and Ballistic free-flight ranges. These are outlined below.

3.2.1 Shock Tubes

A Shock Tube facility is one where a shock wave passes through a test gas, creating a high-pressure/ high temperature environment (Bertin 1994).

This type of facility can be divided into two sections that are initially divided by a diaphragm. One of the sections, known as the "driver" section is filled with a gas at a high pressure. The other section is filled with the "driven" gas at a low pressure. As the diaphragm bursts under the high pressure, the motion of the driver gas causes a shock wave to move through the driven section creating the test flow.

One of the important features of this type of system is that the test time that is created

can be as small as fractions of a millisecond. They are not very useful for the testing of scale models.

3.2.2 Arc-heated Test Facilities

In an arc-heated test facility, the test gas is passed through a high-power electric arc (inside a pressure vessel) and then through a converging/diverging nozzle. This creates supersonic flow, and while the impact pressure and enthalpy that are created are similar to re-entry conditions, the Mach number is generally low.

Arc-heated facilities are important because they can be used to

- Prevent condensation of the test gas during expansion to hypersonic Mach numbers
- To replicate the physical and chemical transformation of air for the study of aerothermodynamics.
- To investigate the internal physical and Chemical changes of materials caused by interaction with the high temperature environment.

Arc-heated test facilities can provide relatively high stagnation pressures for test times greater than a minute.

3.2.3 Ballistic Free Flight Ranges

Range facilities allow for the free flight testing of a subscale model in a controlled environment. This is done by shooting the model at hypersonic velocities through a long range tank. The test gas can also be easily changed to simulate the entry of different atmospheres.

The problem with free flight ranges is that often it is difficult to obtain experimental measurements. In addition to this, the large accelerations that are experienced in

testing mean that the model must be relatively small and simple to cope with the large stresses that would be imposed.

3.2.4 Hypersonic Wind Tunnels

In hypersonic wind tunnels, a test gas is accelerated from a reservoir (at rest) through a converging/ diverging nozzle creating hypersonic speeds in the test section. The acceleration may be assumed to be isentropic.

Hypersonic wind tunnels are often categorised by their run time. Impulse facilities have a run time of 1s or less. Intermittent tunnels have run times that range from a few second to several minutes and Continuous tunnels can run for hours.

Obviously, as the run time of the wind tunnel decreases it becomes harder to take accurate measurements of aerodynamic forces because the model will not meet equilibrium. The accuracy of wind tunnel testing also relies heavily on the quality of the flow.

Hypersonic Wind tunnels are the area of most interest to this report as they have similar characteristics to the USQ Gun Tunnel which has a run time of 25ms.

3.3 The USQ Gun Tunnel

The function of the USQ gun tunnel is to produce hypersonic airflow under controlled conditions. The USQ gun tunnel is capable of producing an 80mm diameter flow, at speeds of up to Mach 7 during a 25ms test time.

3.3.1 Facility Layout

The USQ Gun tunnel is located at the University of Southern Queensland (Toowoomba) campus in the 'S Block' basement.

For descriptive purposes, the Gun Tunnel can be divided into three main sections (this

can be seen in figure 3.2).

1. Reservoir Section (Driver section at high pressure)
2. The tunnel and converging/ diverging nozzle (driven section)
3. The test section and dump tank (initially at low pressure)

The reservoir, or driver section is separated is approximately 3m wide by 0.5m. It is separated from the driven section by means of a steel diaphragm that will rupture at the required pressure. One of these diaphragms before (a) and after (b) a test run can be seen in the figure 3.1. In order to maintain a low pressure in the test section it is sealed using a cellophane diaphragm that is eventually ruptured by the fluid travelling at supersonic speeds.

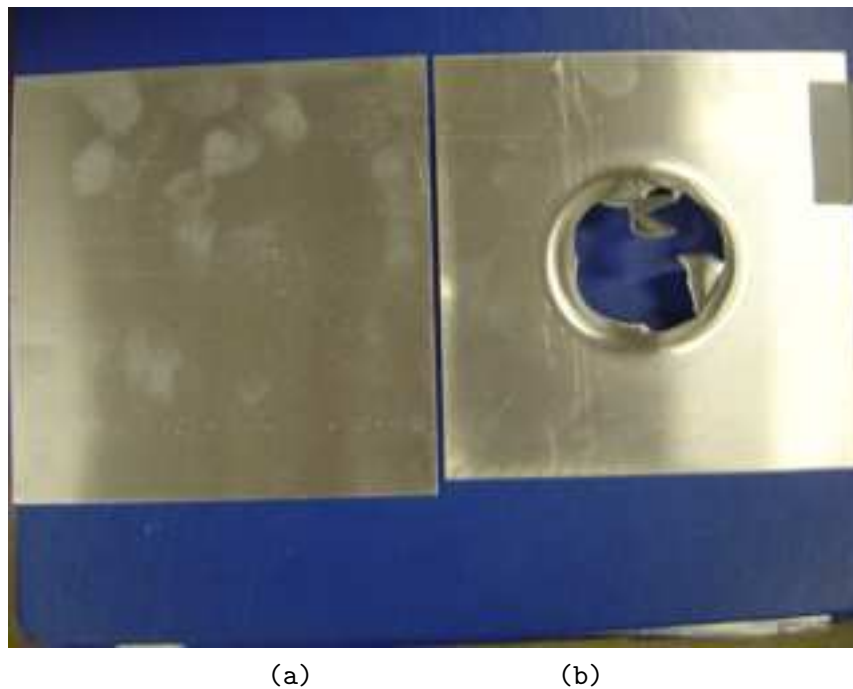


Figure 3.1: Example of diaphragms

3.3.2 Gun Tunnel Operation

For a high pressure test run gun tunnel is operated by pressurizing the driver section reservoir up to approximately 7MPa. When the pressure is sufficient, the 1mm thick

steel diaphragm will rupture allowing the lightweight plastic piston to travel at supersonic speeds (with a shock wave travelling in front of it) down the tunnel, compressing the air in front of it. The tunnel section is approximately 5 meters long and 100 mm in diameter. The fluid is then forced through a converging diverging nozzle, which restricts the flow diameter to 80mm. At the exit of this nozzle is where the fluid is accelerated to velocities of Mach 7 for a run time of up to 25 milliseconds. At the end of the process the air finishes in the dump tank, which is depressurised at the end of the run.

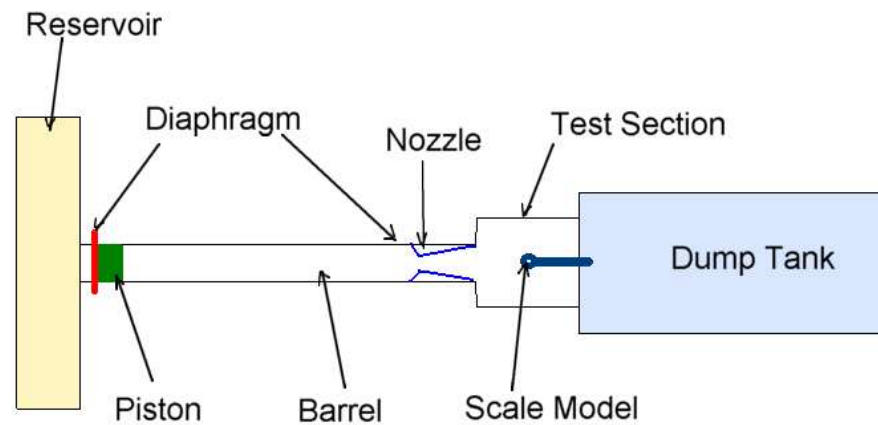


Figure 3.2: Diagram of Gun Tunnel layout

During each test, the stagnation pressure of the flow is measured using a pressure transducer located at the nozzle. Not only is this important for the theoretical force calculations, it also gives an indication of the quality of the flow.

The performance of the Gun Tunnel under high pressure operating conditions can be seen in table 3.1. In this table, free flow conditions describe the actual flow conditions that the model is exposed to. The free flow temperature is very low due to the isentropic expansion that takes place in the nozzle to create hypersonic flow.

Performance Parameter	Value
Mach Number(M)	7
Stagnation Pressure(P_o)	6 MPa
Stagnation Temperature(T_0)	750 K
Free Flow Pressure	1.45 KPa
Free Flow temperature	68.4 K
Initial Density	28.9 kg/m ³
Free Flow Density	0.0753 kg/m ³
Free Flow Velocity	1150 m/s
Pressure Behind the Shock Wave	92.1 kPa
Stagnation Point Pressure Coefficient (C_{pt2})	1.82

Table 3.1: Performance parameters of the Gun Tunnel

3.4 Force Measurement Systems

There are a number of different ways that forces on re-entry capsules can be measured in ground based test facilities. The method of measurement often depends on the performance of the facility itself, but can also depend on the type and accuracy of the data required.

One thing that all impulse facilities have in common is that because of the sudden impact of the aerodynamic forces on the model, the entire system will begin to oscillate at its natural frequency. In a wind tunnel with a reasonable run time, the useful test time would begin after these oscillations had been damped out. However in facilities like the USQ Gun Tunnel with very short test times it is almost impossible to damp out the oscillations and find the steady state. Also, the inertia forces of the oscillating model and balance can add to the aerodynamic forces and moments.

In the past, measurement of aerodynamic forces in short duration test facilities has been restricted because of the time that it takes for the model to reach equilibrium with its support mechanisms. Force balances often rely on damping mechanisms or filters to reduce the effects of the vibrations that are caused by the sudden impact of the aerodynamic force (Mee 2003). Unfortunately at times the test time of the flow may be too short to damp out these vibrations and in some cases the period of oscillation of the model can be longer than the actual test time.

A number of techniques can be used to fix this problem. The natural frequency of the system can be increased by making the force balance very stiff and the model very light. Another option is to use accelerometers that can be placed on the model to detect vibrations and compensate for the strain signals from the force balance. Alternatively the model could be connected with flexible supports and its acceleration measured. This can then be taken one step further and the model be allowed to 'fly free' during the test. This removes the effect of the support mechanism that decreases the natural frequency of the system. In the case of the free flying model, the natural frequency would be set only by the model size and the speed of the stress waves in the structure of the model (Mee 2003).

A method was developed to measure the acceleration of a free flying model in a shock tunnel (Störkmann 1998). The model was controlled by a mounting support that releases the model just before the onset of the flow. During the test there are no connecting parts between the model and the support system. The support system does not cause the model to accelerate. The forces are then determined from the accelerations and inertia matrix of the model using Newton's Law. In this test it is essential to have the model equipped with at least six accelerometers. Hence this would be a very expensive system to set up.

The method that Mee used for force measurement in impulse test facilities involved the connection of the model to a long hollow sting (Störkmann 1998). The setup hangs in the wind tunnel from two shielded wires that can freely move in the flow direction. In this case the stress waves that are introduced into the system are measured, rather than the acceleration. The setup can be seen in figure 3.3.

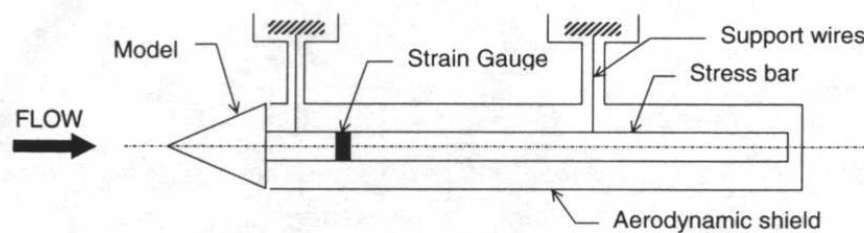


Figure 3.3: Single-component stress-wave force-balance (Mee 2003)

An alternative method has been used in the SR3 wind tunnel. The SR3 wind tunnel generates hypersonic nitrogen flows for a continuous run time. Hence it will not experience many of the difficulties associated with impulse facilities, however it is still worth investigating. The force balance that is used in this case is connected by two wires and utilizes three dynamometers to take measurements. This system allows for the measurement of drag, lift pitching moment and centre of pressure with good accuracy. Unfortunately this does not address the problem of the oscillation of the model because the measurements at the SR3 wind tunnel can be taken over a few seconds.

A force balance that is similar in nature to the one at USQ was designed by Jessen and Grönig (this is described in (Störkmann 1998)). They use a strain gauge balance that is designed to work without any acceleration compensation. The balance is part of the sting (or mounting arrangement) and is essentially independent of the model. In this case, no acceleration gauges would be needed inside the model. This system can be calibrated statically with high accuracy and achieves a high natural frequency in excess of 1kHz.

After examining this system and its test results it is concluded in (Störkmann 1998), that it is possible to determine aerodynamic loads without without compensation for the inertia forces caused by the oscillation of the model and support system. That is, provided the measurement time is longer than the lowest natural frequency of the system-model balance. If the system is optimised in terms of weight and moment of inertia to give a higher natural frequency, it will give more reliable measurements.

3.4.1 Calibration

In his paper, Mee discusses the calibration of force balances for hypersonic test facilities. This calibration can be performed either by a *hung weight test* (that will be described in chapter 5), a self weight test, or a hammer pulse test. All these techniques have the same underlying principle; by applying a known load, the response of the system can be modeled.

An important point that Mee makes is that calibrations should be performed when

the model is mounted in the test tunnel. This way, the characteristics of the tunnel mounting arrangement can be included in the model response.

3.5 The USQ Force Measurement System

The current design of the force measurement system can be seen in figure 3.4, which includes the mounting plate and sting. The model of the entry capsule is connected to the sting, which is a bar that connects the model to the mounting arrangement in the Gun Tunnel. The sting consists of a 20mm steel bar joined to an Aluminium I-Beam. It can be seen (in figure 3.4) that the angle of attack of the capsule can be changed depending on how the sting is mounted. It can be adjusted between -20 and +20 degrees. In this system, the aluminium I-beam is protected by a stainless steel sleeve. This is important as the I-beam holds the measurement apparatus.

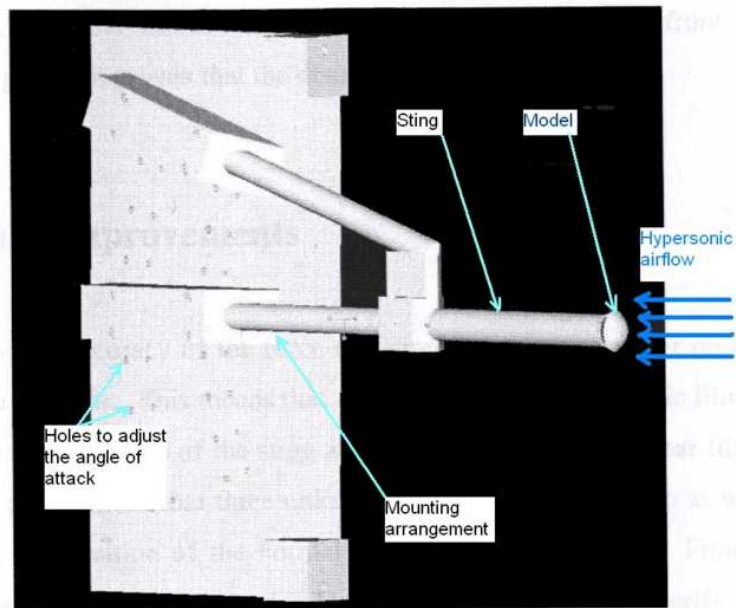


Figure 3.4: The existing mounting arrangement

The way that this system works, is that the force acting on the entry capsule is transferred through the I-beam. By measuring the strain on this cantilever we can then estimate the forces acting on the capsule.

The system can be described by figure 3.5. In this diagram it shows that if a load is

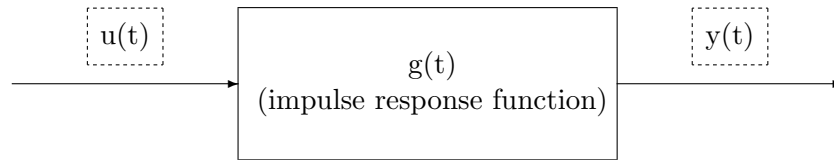


Figure 3.5: System description

applied ($u(t)$) then the output of the system ($y(t)$) will be value of strain according to the impulse response function. Therefore if we can determine this function (through calibration) then we can use a measured value of strain to find the applied load.

The strain is measured using piezoelectric films as strain gauges. Two of these films were bonded to the top surface of the I-Beam. When the beam is loaded a voltage difference is created across the film. This change in voltage is directly proportional to the strain. By using the correct calibration process the strains on the I-Beam cantilever can be accurately determined and hence the forces on the re-entry capsule measured.

3.5.1 Measurement of Strain

Piezo films typically produce a charge in the order of 10 nano coulombs (depending of the strain that they are subjected to). From this it is obvious that some type of amplification equipment will be required. The other thing that must be realised is that the charge on piezo films is directly proportional to the change in strain. Therefore if the load is not changing the voltage output of the film will die fairly rapidly.

Equipment that is required to actually record these measurements included;

- Conditioning amplifier: The output of the piezo-electric film is connected directly to the *Bruel & Kjaer* conditioning amplifier. The output of this amplifier will be 3.16V per nanoCoulomb.
- Oscilloscope: This receives the signal from the amplifier and is used to capture

the data from the test run.

- *Wavestar* computer software: This takes the data from the oscilloscope and compiles it in tabular form. This allows for further analysis of the results

3.6 Chapter Summary

This chapter gave an overview of why ground based testing is important and looked into various hypersonic test facilities. It also gave an overview of some existing hypersonic force measurement systems.

In this section, a description was given of the USQ Gun Tunnel and how aerodynamic forces are measured at hypersonic speeds in this facility.

Chapter 4

Analysis of Original System

4.1 Chapter Overview

In order to improve the existing force measurement system that is employed in the USQ Gun Tunnel, it is important to know how the system works. Before any improvements can be made, the system must be analysed to identify any problems and areas that require modification.

This chapter will look at the results of the initial system and describe the ways that these could be improved.

4.2 Original Results

The results that were obtained from previous measurements from a high pressure test run (at Mach 7) in the Gun Tunnel, with an angle of attack of 10 degrees indicate normal forces of 0.927N and Axial forces of 72.9N (Terhorst 2001).

As there are only two strain gauges, one located at the front of the I-Beam and one at the back hence only two unknown variables can be found. Therefore, with the current system, the position at which the forces will act on the model must be estimated when

calculating the normal and axial forces. This location where the forces are assumed to act is known as the centre of pressure.

As previously mentioned when the forces are determined for the entry capsule there is not one steady force (or voltage) that is measured. Instead the whole system will oscillate at the natural frequency of the arrangement. This means that an average value of the force must be taken over a period of time. The time span where there is a constant pressure exerted in which to take measurements will be 25ms at best.

The test run used by Terhorst(2001) to obtain his measurements provided good flow conditions for 20ms. However the force measurement system provided useful measurements for only 4 milliseconds, (from 23 milliseconds to 27 milliseconds) as can be seen in figure 4.1). After this period the output is less useful and appears to be affected by resonance or a second lower frequency. This may be improved by some type of damping system. The frequency of the system in the hypersonic flow was determined to be 500 Hz (Terhorst 2001, pg. 81).

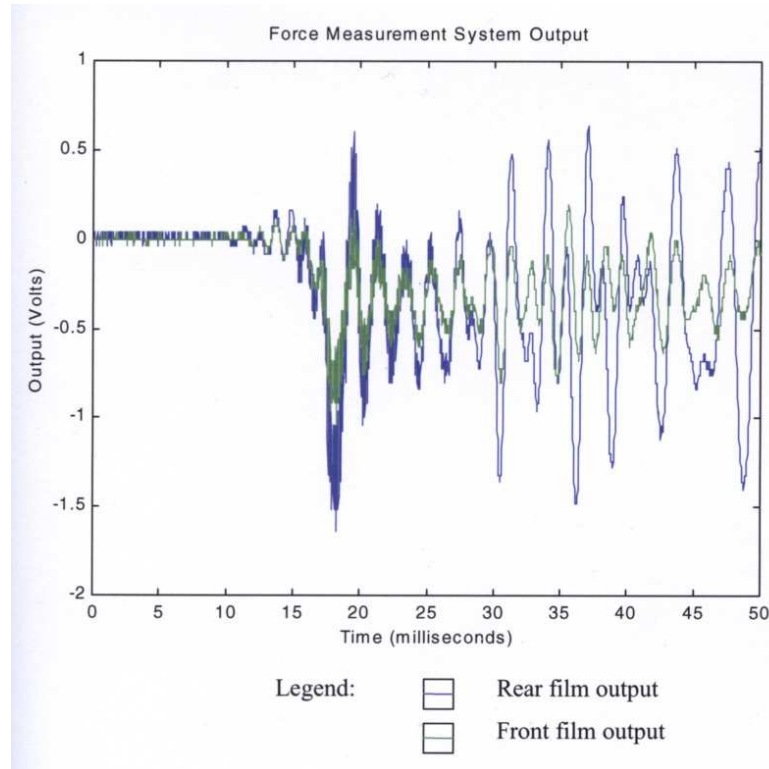


Figure 4.1: Results of the previous Force Measurement System

4.2.1 Expected Results

The theoretical values obtained for these forces were 8.2185 N in the normal direction and 78.3808N in the Axial direction. This can be compared to the measure values of 0.927N in the normal direction and 72.9N in the axial. From this data it can be seen that the force prediction is reasonably accurate in the axial direction, however the error associated with measuring normal forces is significant.

The results of this system for a high pressure test run can be seen in the table below. This will be important in designing the system, in terms of the magnitude of the strain that will need to be measured for a given configuration.

Angle of Attack (Degrees)	Axial Force (Newtons)	Normal Force (Newtons)
0	80.0709	0.0000
2.5	79.9642	2.0936
5	79.6451	4.1712
10	78.3808	8.2158
20	73.5143	15.4406
-20	73.5143	-15.4406
-10	78.3808	-8.2158
-5	79.6451	-4.1712
-2.5	79.9642	-2.0936

Table 4.1: Expected forces in high pressure Gun Tunnel test (at Mach 7)

4.3 Bench testing of original system

A simple program of bench testing was undertaken with the existing system to see how the dynamics on the model could be changed.

4.3.1 Method

This testing was not performed in the Gun Tunnel hence the actual values that were obtained are of no particular significance. The point of this exercise was to determine

how the natural frequency and damping properties of the sting/model system changed as certain modifications were made.

For these tests the sting was clamped to a bench using two G-clamps. The model was excited by being gently struck with a rigid object. The response of the system was observed through the oscilloscope.

The original configuration was compared to a system where the I-beam was damped by oil. Different methods of joining the back of the model to the protective sheath were tested. These included *Blu-Tac*, tape and cardboard. All of these modifications were an attempt to improve the original system which had no damping mechanism.

For each test the natural frequency was determined and the damping ratio calculated. The most convenient way to determine the amount of damping present in the system is to measure the rate of decay of free oscillations. Obviously, the more damping there is, the larger the rate of decay. The natural logarithm of the ratio of two successive amplitudes is known as the logarithmic decrement, δ . This can be determined using equation 4.1, where $\frac{X_1}{X_n}$ is the ratio of the amplitude of oscillations over n cycles.

By using the experimental values, (an example of which can be seen in figure 4.2) and equations 4.1 and 4.2 (W.T.Thomson 1988, p .33) we can determine the damping factor, ζ . The ideal system would be critically damped, $\zeta = 1$. However, from the existing results of the measurement system, it is obvious that the existing system is underdamped, meaning $\zeta < 1$.

$$\delta = \frac{1}{n} \ln\left(\frac{X_1}{X_n}\right) \quad (4.1)$$

$$\zeta = \frac{1}{\sqrt{1 + (2\pi/\delta)^2}} \quad (4.2)$$

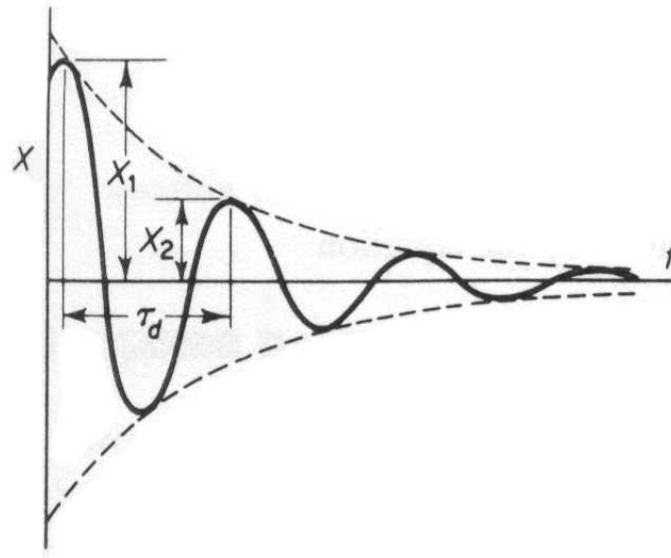


Figure 4.2: Rate of decay of oscillation measured by the logarithmic decrement (W.T.Thomson 1988, p. 33)

4.3.2 Summary of Results

A summary of the results of bench testing of the existing system can be seen in table 4.2. From this data it can be seen that there is a clear trend.

- As the damping of the system is increased the damped natural frequency is reduced.

This is shown by equation 4.3 where an increase in ζ would cause the damped natural frequency to decrease.

$$\omega_d = \omega_n \sqrt{1 - \zeta^2} \quad (4.3)$$

While the natural frequency is reduced significantly, the value of the damping factor remains quite low. Even with the addition of the oil damping, the system is still far from being critically damped.

It must be noted that when the protective sheath was filled with oil, a second lower natural frequency ($\approx 250Hz$) became obvious. This is important because it is the

lowest natural frequency of the system that is important when trying to increase the accuracy of measurements (Chapter 3.4). The oil appeared to damp out the higher frequency vibrations.

Fluid surrounding I-Beam	Sealing Method	Natural Frequency (Hz)	Damping Factor
Air	-	500	0.02
Air	<i>Blu-Tac</i>	416	0.03
Oil	-	263*	0.09
Oil	<i>Blu-Tac</i>	250	??
Oil	Tape	240	0.14

Table 4.2: Summary of Initial Bench Testing

During this testing it became obvious that the piezo-electric films were susceptible to interference. At times the output was effected by mains power (in the form of a 50 Hz frequency) and even the movement of bodies around the model. This is one area that would need to be addressed as it could have significant effect on the results.

4.4 Use of Piezoelectric Strain Gauges

The accuracy of the films has a large bearing on the accuracy of the force measurement system as a whole. Therefore it is important to understand the limitations and possible sources of error when using this equipment.

The use of piezoelectric films as strain gauges for the USQ Gun Tunnel has a number of advantages. They can be easily cut to any size and bonded using commercially available adhesives. More importantly, they are small and very light and can therefore be attached to the system without effecting its dynamic properties or the motion of the device. Piezo films also have a high mechanical strength and impact resistance. Combined with this they have high stability, resisting most chemicals, moisture and ultra violet radiation.

Piezoelectric films also have a wide frequency range (0.001 Hz - 1GHz) and large dynamic range suitable for measuring strains from $0.1 \mu\epsilon$ to $800 \mu\epsilon$.

4.4.1 Material Properties

Piezoelectric films are polymer films based on polyvinylidene fluoride (PVDF) that have piezoelectric properties that enable them to be used as electromechanical transducers. They are particularly useful as dynamic strain sensors

The actual strain gauge is formed from a piece of this piezo film (20 - 50microns thick) that has been metalised, and uniaxially oriented.

The piezoelectric films that have been used at USQ have a piezoelectric strain constant of $69 \times 10^{-3} C/m^2$. This can be used to estimate the charge that will be created by a certain strain.

$$\text{Charge, } Q = \text{Area of Film} \times \text{Strain} \times \text{constant} \quad (4.4)$$

It has been shown that piezoelectric films exhibit a linear response to strains of up to $800 \mu\varepsilon$.

The strain gauge is glued to one side of the component and the charge output is found by connecting insulated wires to either side of the film (as can be seen in figure 4.3). These wires can then be connected to a charge amplifier and the output voltages can be viewed from an oscilloscope.

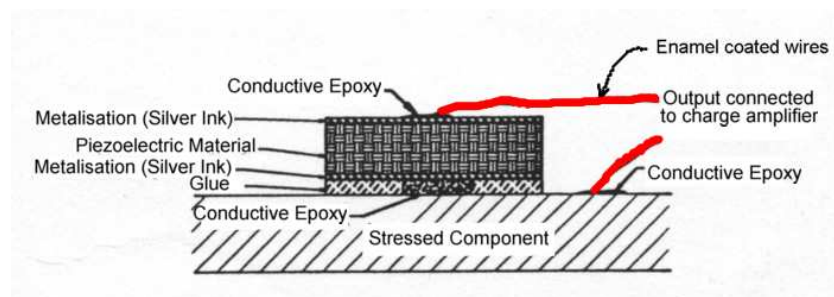


Figure 4.3: Cross section of piezoelectric strain gauge. (Smith p .7)

Piezoelectric films can only be used for dynamic (i.e. changing) strain measurement. The charge is generated as a result of the actual change in mechanical strain.

4.4.2 Problems with Piezoelectric Strain Gauges

While the use of piezoelectric films as strain gauges offers a number of advantages, there are also a few problems. These include,

- High sensitivity to changes in temperature: This must be considered, particularly if the film is exposed to the flow stream.
- Can be sensitive to electromagnetic radiation/interference (EMI): This may become a problem if the output level of the films becomes too small.
- AC Mains interference can be a problem with unshielded devices.

In order to improve the accuracy of results, these problems must be considered.

4.5 Required Areas of Improvement

From the analysis of the system it can be seen that there are a number of areas that require improvement in order to increase the accuracy of the forces measured.

The first problem that has been identified is that the centre of pressure needs to be identified through measurement, rather than estimation. This would reduce some of the errors associated with the force calculation.

Secondly, the natural frequency of the model needs to be improved to increase the number of oscillations in the measurement period. Ideally the natural frequency should be above 1kHz. This value was achieved by Jessen and Grönig (see chapter 3.4) and should be acceptable.

In addition to these improvements it would be desirable to improve the damping properties of the system. As it was seen in the initial bench testing, the system was under-damped (table 4.2).

It was also noted that the piezoelectric films used for strain measurement were suscep-

tible to background interference and were very sensitive to changes in temperature. In order to get the most out of this system it is crucial that the effect of these external influences are minimised.

4.6 Chapter Summary

This chapter has examined the current results of the USQ force measurement system and compared them to expected outcomes. Some simple bench testing was undertaken to characterise the dynamics of the original system. At the same time the original system was modified to try and improve damping properties and natural frequency. Using the gathered information conclusions were drawn about the required areas of improvement.

These were:

1. The centre of pressure must be identified.
2. The natural frequency of the system must be increased.
3. The damping properties of the system should be improved.
4. The accuracy of the piezoelectric films should be improved through the reduction of background interference.

Chapter 5

Improvement of the existing System

5.1 Chapter Overview

This chapter will look at how to improve the USQ force measurement system in the ways that were identified in chapter 4. These improvements will then be implemented in the new design of the USQ Force measurement System which will be bench tested to ensure the accurate measurement of strain in the cantilever.

5.2 Method of Improvement

5.2.1 Improving the Frequency Response

Some simple methods are to:

Decrease the mass of the model and/or cantilever. This might be done by using different materials or reducing the amount of material used in the sting. Lighter metals or fiber composites could be investigated. The effect of change in mass on the natural frequency of the cantilever system can be seen in figure 5.1, where a 50 percent reduction in the

mass of the entry capsule creates only a 30 percent increase in the natural frequency of the system. This graph assumed the system was a uniformly loaded beam with a mass located at the end. (This is further discussed in chapter 5.3.1)

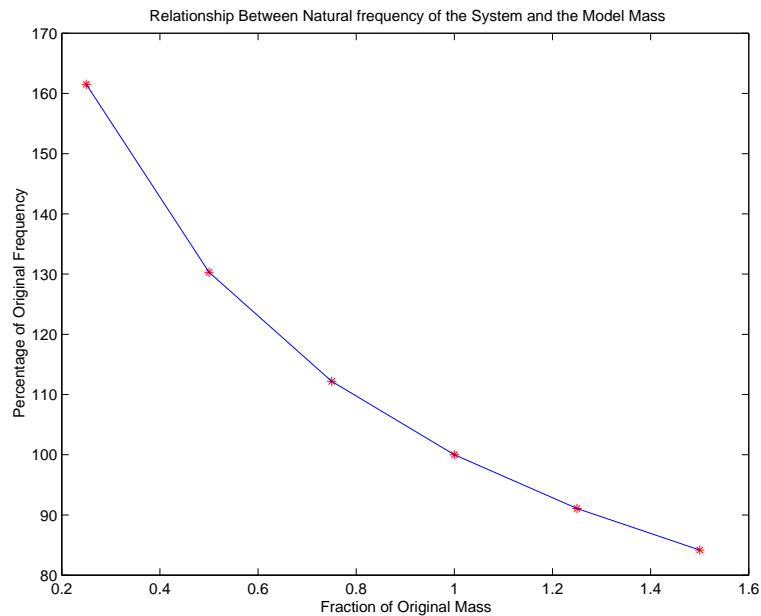


Figure 5.1: Graph showing the effect that changing the mass of the model has on the frequency of the system

Decrease the length of the cantilever. By decreasing the overall length of the cantilever, the stiffness of the sting will be increased and hence the frequency of oscillation will increase. This would be one of the easiest ways to increase the natural frequency as it also reduces the mass of the cantilever. The effect of the change in length of the I-Beam can be seen in figure 5.2, where a 50 percent decrease in length will cause the frequency to increase by almost a factor of three.

Increase stiffness of the section. This could be done by either shortening the cantilever as previously stated, or by changing the section properties or material properties. The existing system is quite good, with the I-Beam being one of the best options in terms of the stiffness to weight ratio. Terhorst (2001) attempted to increase the stiffness by adding bracing to the final design. This worked well, but something more effective is required.

Essentially what is required, is the stiffest section with the least weight in order to produce a high natural frequency in the force measurement system. This is where one

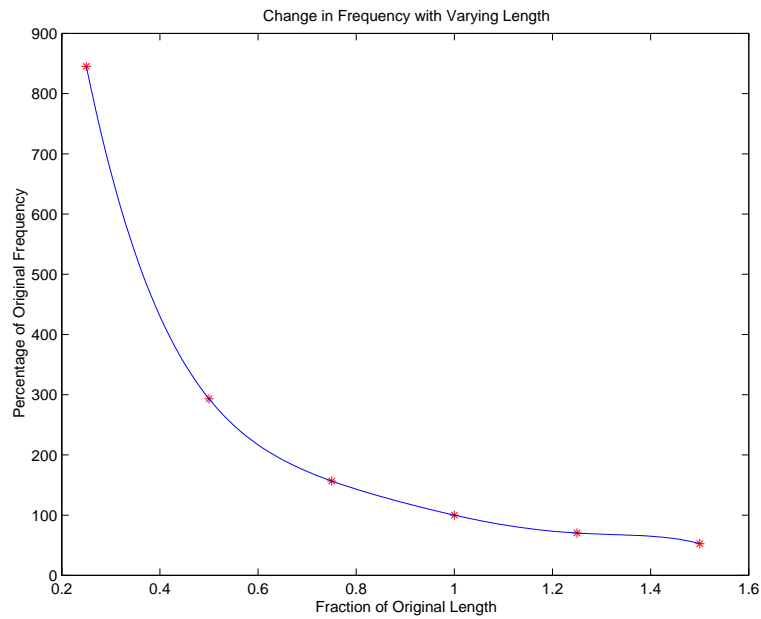


Figure 5.2: Graph showing the effect that changing the length of the cantilever has on the frequency of the system.

of the problems lies. It is desirable that the sting is as stiff as possible in order to give high natural frequencies, however the basis of the system is the measurement of the strains in the cantilever beam. This means that if the sting is made too stiff, the strains imposed on the cantilever will be too small to accurately measure. Therefore, the minimum strain measurement must be determined and the system designed around this.

The entry capsule model and sting assembly is made from Aluminium. In designing the force measurement system we require as high a natural frequency as possible. For the cantilever, a material was required that was lightweight and also stiff. Aluminium was previously chosen as the best, however a number of other materials were investigated. Table 5.1 shows the change in natural frequency of the existing system design if new materials are used. A value greater > 1 in the far right column would indicate an increase in the natural frequency.

It must be realised that if the section is made too stiff then the strains that will be measured will be too small and then the effect of background noise/interference will be greater. In addition to this if the actual section is made too short, the piezoelectric films will have to be made very small. It was shown in equation 4.4, that the charge that is

Material	Density, ρ (kg/m^3)	Modulus of Elasticity, E (Pa)	Natural Frequency, f_n (Hz)	Frequency compared to aluminium ($\frac{f_n}{f_{n(A)}}$)
Aluminium	2700	7.00×10^{10}	744.81	1.0000
Steel	7700	2.07×10^{11}	759.83	1.0186
Titanium Alloy	4400	1.14×10^{11}	745.94	1.0015
Brass	8300	1.10×10^{11}	533.51	0.7163
Zinc Alloy	6600	8.30×10^{10}	519.69	0.6978

Table 5.1: Effect of alternative materials on the natural frequency

produced by the piezoelectric strain gauge is directly proportional to its area. Hence the use of smaller films would lead to a smaller charge output. This would increase the effect of background noise.

From the information presented here, it can be seen that the most logical way to increase the natural frequency of the system is to reduce the length of the aluminium I-Beam. By changing materials there is no real advantage gained. The reduction of the mass of the model would cause some increase in natural frequency, however the reduction in the length of the cantilever appears to be the best option. If its length is halved, the natural frequency should be approximately increased by a factor of three almost (figure 5.2).

5.2.2 Improving the Damping Properties

The improvement of the damping properties of the sting will help to give clearer results which will in turn make analysis easier.

Simple experiments were performed on the existing model to calculate the damping factor, which was in the order of 10^{-3} . A critically damped system has a damping factor of one, which indicates the current system is extremely under-damped and there is significant room for improvement. The damping properties could be improved by connecting the back of the entry capsule model to the protective sleeve with a flexible connection.

Another method is to fill the protective sleeve with oil, which would be sealed at the

back of the entry capsule. This would mean the entire I-Beam was submerged in oil. It was shown that this did increase damping, but not significantly. This would have to be set up very carefully to ensure the surrounding fluid does not affect the strain gauge measurements. The use of oil might also offer some advantages in terms of reducing the heating effects on the strain gauges.

Bench testing revealed that while the use of oil as a damping mechanism did increase the damping factor in comparison to the undamped system, it didn't offer any real advantage to the system. This was because the damping factor still remained quite low. If anything, the addition of the oil would cause problems in trying to keep the system sealed. Leaking would be a problem where the wires exit the protective sheath.

There will be some type of flexible connection between the model and protective sleeve (probably electrical tape). This may improve damping properties slightly, but its primary use is to prevent any of the flow getting to the piezo films. Hence this would also eliminate any temperature effects. This is an improvement on the original system, and will help to ensure that the piezoelectric films are not influenced by temperature changes during the test.

5.2.3 Improving the Piezoelectric Output

As was noted earlier the piezoelectric films were susceptible to interference. This problem was compounded by the fact that the power for S-Block runs through the basement where the Gun Tunnel is located. With the existing system, the films were bonded to the sting using a conductive epoxy. This meant that there was a very large metal area that was connected to the piezoelectric films that also had the ability to increase the amount of interference that was received.

Initially an attempt was made to improve the piezoelectric film application procedure. The idea of this was to make the piezo film and its wires a discreet system, such that it was glued to the I-Beam but in no way electrically connected. This would hopefully reduce the amount of interference that could influence the measurements. The basic procedure that was followed was:

1. Bond wires to both sides of the Piezoelectric film using a conductive (silver based) epoxy.
2. Cover the conductive epoxy on the underside with tape to prevent electrical contact with the stressed member.
3. Then bond the piezoelectric film to the stressed member using araldite.

The idea with this was that the araldite would prevent a connection between the film and the I-Beam. However this was not the case and contact was still made. This could probably be prevented by applying tape to the entire underside of the piezoelectric film, but this would compromise the strength of the bond between the film and the stressed member.

The other option was to shield the device. This was investigated during the bench testing where aluminium foil was used to shield the wires and the sting/model system. It did make a considerable difference, but when moved to S-Block the 50Hz frequency of the mains power was still an issue. However once the model was actually mounted in the test section of the Gun Tunnel, the problem was removed. Presumably the 10mm thick steel that forms the test section acted as a shield.

This means that while the attempt to improve the application procedure of piezoelectric strain gauges didn't succeed, accurate measurements can still be taken provided the model is either shielded with aluminium foil or preferably is mounted in the Gun Tunnel.

5.2.4 Accurately Determining the Centre of Pressure

When estimating the force acting on a surface due to a certain flow, the pressures and shear stress over the surface can be integrated over that surface to give a resultant force (R). This force can be assumed to act at the centre of pressure of the model. Figure 5. shows a typical location of the centre of pressure (cp) with the Normal(N) and axial(A) components of the resultant force (R). The location of the centre of pressure is described by x_{cp} and y_{cp} . This diagram shows a pointed cone body shape, however the principle is the same for blunted bodies like MUSES-C.

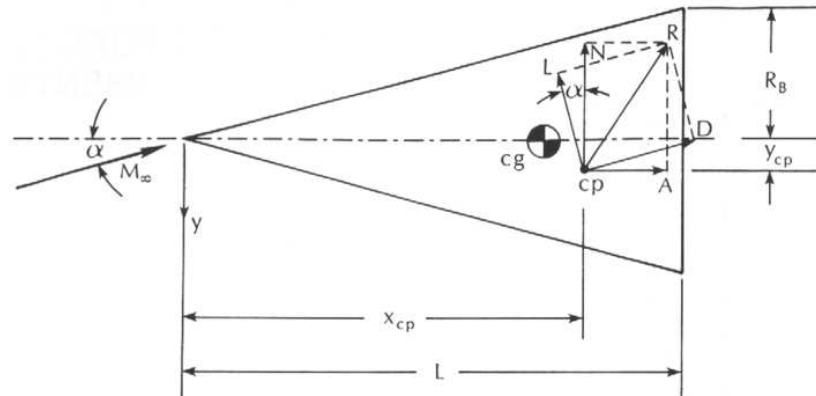


Figure 5.3: Location of the centre of pressure
(Bertin 1994, p. 442)

One major area of improvement is to modify the force measurement system so that the centre of pressure location can be determined and the normal and axial forces are predicted accurately.

The simplest way to do this is to use more strain gauges. The addition of an extra film on the underside of the I-Beam would allow for the centre of pressure to be identified, however a fourth strain gauge would be ideal. This would allow for the identification of the exact location of the centre of pressure.

5.3 Design of the New System

Taking into account the required areas of improvement and the various ways to make these improvements, a new system was designed. This adopted the features of the old system, but with a few simple changes.

- The length of the Aluminium I-beam was reduced by 40mm. This is approximately half of the original length and should lead to a significant increase in the natural frequency of the system. The new component is shown in figure B.1.
- Four Piezoelectric films were applied to be used as strain gauges. These piezo films are roughly the same size of as the original ones ($10 \times 20mm$) and are located on the top and bottom of the aluminium I-beam.

- The protective sheath was changed to a suitable length and will be connected to the model using electrical tape to reduce any flow effects on the piezoelectric strain gauges.

The new system setup can be seen in figure 5.4. (The protective sleeve has not been put on in this picture to allow the position of the strain gauges to be seen.)

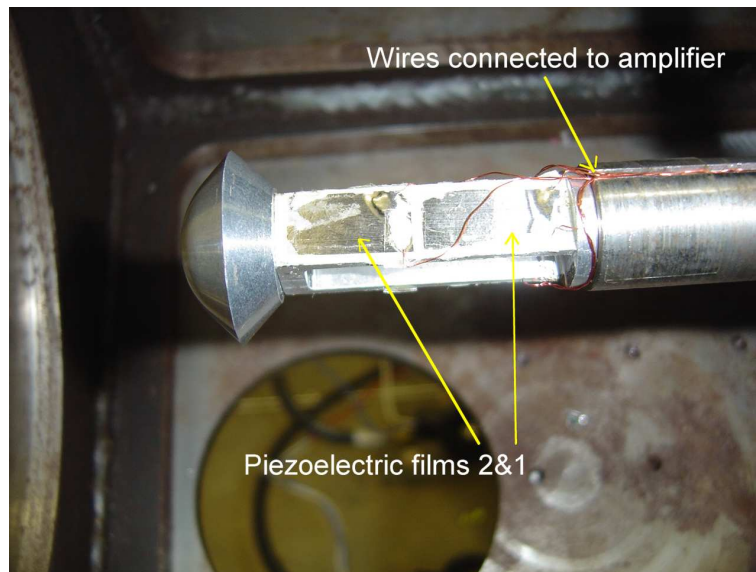


Figure 5.4: New system setup (with piezoelectric strain gauges)

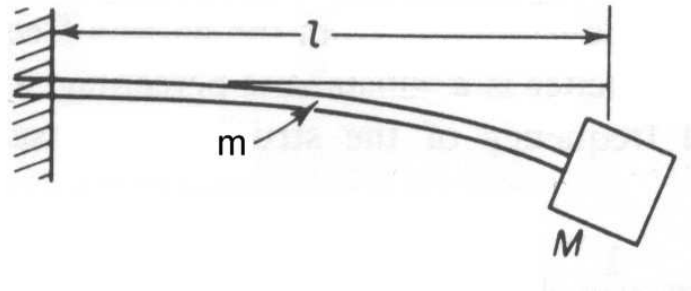
5.3.1 Frequency Prediction

With the new system specified it is important that its natural frequency is modeled to ensure it will be suitable.

An appropriate way to do this is to treat the system as a uniformly loaded beam with a mass located at the end (see figure 5.5).

The frequency for this system can be modelled by looking at the effect of the model and the beam separately.

The cantilever I-beam will be looked at first. The frequency of the cantilever beam is calculated using equation 5.1 (W.T.Thomson 1988, p. 302)



(W.T.Thomson 1988)

Figure 5.5: Sketch of how the system will be modelled for natural frequency prediction

$$\omega_{11}^2 = 3.515^2 \left(\frac{EI}{ml^3} \right) \quad (5.1)$$

The frequency of the model, of mass M , can be found with equation 5.3

$$\omega_{22}^2 = 3.00 \left(\frac{EI}{Ml^3} \right) \quad (5.2)$$

These can then be combined using Dunkerley's formula (W.T.Thomson 1988, p. 302) to find the overall natural frequency, ω_1 .

$$\omega_1^2 = \frac{\omega_{11}^2 \omega_{22}^2}{\omega_{11}^2 + \omega_{22}^2} \quad (5.3)$$

Using this process the natural frequency of the system can be estimated to be 1925 Hz. This appears to be quite high, however the natural frequency will probably be a bit lower than this as the I-beam is not mounted on a rigid fixture. Even though the steel bar it is connected to is well braced, it will still decrease the natural frequency.

5.3.2 Piezoelectric Accuracy

It is crucial that the piezo electric films are being used to measure stresses that are within their linear operating range. To check this, the output of the films can be calculated for their worst loading cases.

It was previously stated that the piezoelectric output would measure strains as small as 0.1 microstrain. This lower limit is set by the noise from the piezoelectric element and its hardware. This value of strain can be applied to the new system to determine the accuracy to which forces can be measured.

For this calculation, the piezoelectric films closest to the model will be used as these will record the smallest values of strain. This is due to the smaller bending moment at the closer strain gauges which is associated with any normal force. It was found that a normal force of 0.14N would produce the minimum value 0.1 microstrain.

The system will also be checked for the axial force that would be required to generate 0.1 microstrain. The force needed for the minimum strain measurement is 0.45N which is larger than the force required in the normal direction. It can be seen from this, that the force measurement system will at best measure forces to an accuracy of 0.45N. This should be acceptable.

It was also noted previously that the piezoelectric films would behave linearly up to 800 microstrain. Therefore we must check that in the maximum loading conditions this value of strain is not reached. The largest strains will be experienced at the largest angle of attack due to increased bending stresses. It was estimated that at an angle of attack of 20 degrees during a high pressure run, the forces present would be:

- Normal Force = 15.4 N
- Axial Force = 73.5 N

This can be considered as the worst load case, in which the maximum stresses will exist at the piezoelectric films at the rear of the I-Beam (furthest away from the model). The stresses that will be experienced here will be approximately 3.5MPa which will cause a strain of $50\mu\epsilon$. This is well below the maximum value of strain.

These calculations show that relationship between the applied force and the piezoelectric output will remain linear during high pressure hypersonic tests in the USQ Gun Tunnel. The system will also support larger models without reaching the maximum

strain value. It was seen that a reasonable accuracy was maintained with an error in the order of 0.5N

5.4 Bench Testing the New System

The system was initially bench tested to ensure the piezoelectric films were all functioning correctly. This allowed for the performance of the system to be assessed before the model was put into the gun tunnel.

5.4.1 Initial Calibration of Piezoelectric Films

It is known that any force acting on the model will create a strain in the beam it is mounted on. This strain can be measured using piezoelectric films and as a result the force can be determined. However to measure the strain present, the relationship between the output charge of the piezo film and the applied strain must be determined. This relationship can be found theoretically, but can be more accurately determined through calibration. The system will be calibrated by applying certain forces and then recording the output of the piezoelectric films. These forces were applied using weights which were rapidly released from the end of the cantilever to create a step input.

The calibration data for one piezoelectric film can be seen in table 7.1. The centre of this piezoelectric film is located 34.75mm from the end of the cantilever, where the force is applied.

For all calibrations the charge amplifier was set to $\left(\frac{3.16}{3}\right) \frac{V}{nC}$.

The measured values were then graphed to determine the actual sensitivity of the strain gauge. It can be seen from the slope of the graph in figure 5.6, that the piezo film will produce 14.165mv per microstrain. This graph shows that there is a linear relationship between the strain and the piezoelectric output and that forces can be calculated accurately using this system (as indicated by the R^2 value close to 1). The R^2 value is known as the coefficient of determination, and is an indication of the

Mass (kg)	Force (N)	Stress (MPa)	Strain $\times 10^6$	Measured Voltage (mV)
0.0000	0.000	0.000	0.000	0
0.6160	6.043	0.968	13.83	198
1.1200	10.99	1.760	25.15	360
1.6160	15.85	2.540	36.28	524
2.1200	20.80	3.332	47.60	664

Table 5.2: Important values for calibration of a piezoelectric strain gauge

strength of the linear relationship between strain and the output voltage. A perfect correlation would have an R^2 value of 1.0.

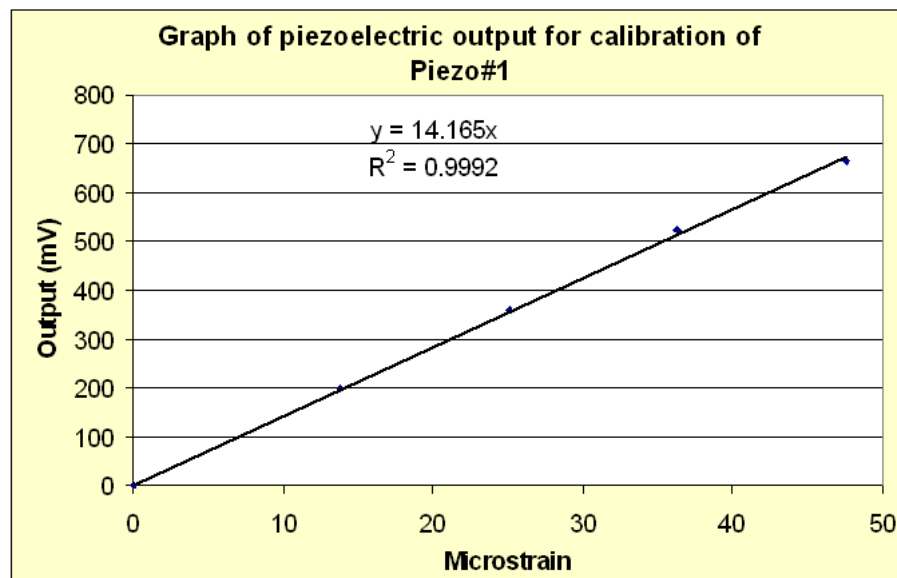


Figure 5.6: Graph used for calibration of piezoelectric films

This process was repeated for all four piezoelectric films and all exhibited similar properties. Even though the sensitivity of some of the films was different, the degree of accuracy was much the same with a very strong linear relationship between strain and measured voltage.

5.4.2 Expected Piezoelectric Output

The expected sensitivity of the piezoelectric films can be calculated using equation 4.4.

For a value of $1\mu\epsilon$ with the piezo film area of $2 \times 10^{-4}m^2$ the expected charge will be.

$$\begin{aligned}
 \text{Charge} &= 1E^{-6} \times 2 \times 10^{-4} \times 69 \times 10^{-3} \\
 &= 1.38e^{-11} \text{ Coulombs} \\
 &= 0.0138 \text{ nC}
 \end{aligned}$$

Because the charge amplifier is set to $\left(\frac{3.16}{3}\right) \frac{V}{nC}$, the voltage that will be produced by this charge is;

$$\begin{aligned}
 \text{Voltage} &= \left(\frac{3.16}{3}\right) \times \text{charge} \\
 &= 0.0145V \\
 &= 14.5 \text{ mV}
 \end{aligned}$$

Therefore the piezoelectric films should produce $14.5 \frac{mV}{\mu\varepsilon}$. This is very close to the results that were found during the calibration of the first piezoelectric film. The sensitivity of the other piezoelectric films were; $11.0 \frac{mV}{\mu\varepsilon}$, $14.9 \frac{mV}{\mu\varepsilon}$, $16.9 \frac{mV}{\mu\varepsilon}$. These also are reasonably close to the expected values.

This initial bench testing has shown that the Piezoelectric films are working accurately and are producing charges very close to the theoretical values.

5.4.3 Frequency Response

The natural frequency of the new system was also tested. This test was performed in the USQ Gun Tunnel.

In the first case (see figure 5.7) the natural frequency was seen to be approximately 1.1kHz.

When the model was taped to the protective sheath the frequency remained virtually unchanged. Figure 5.8 shows the frequency response of the model with tape connection

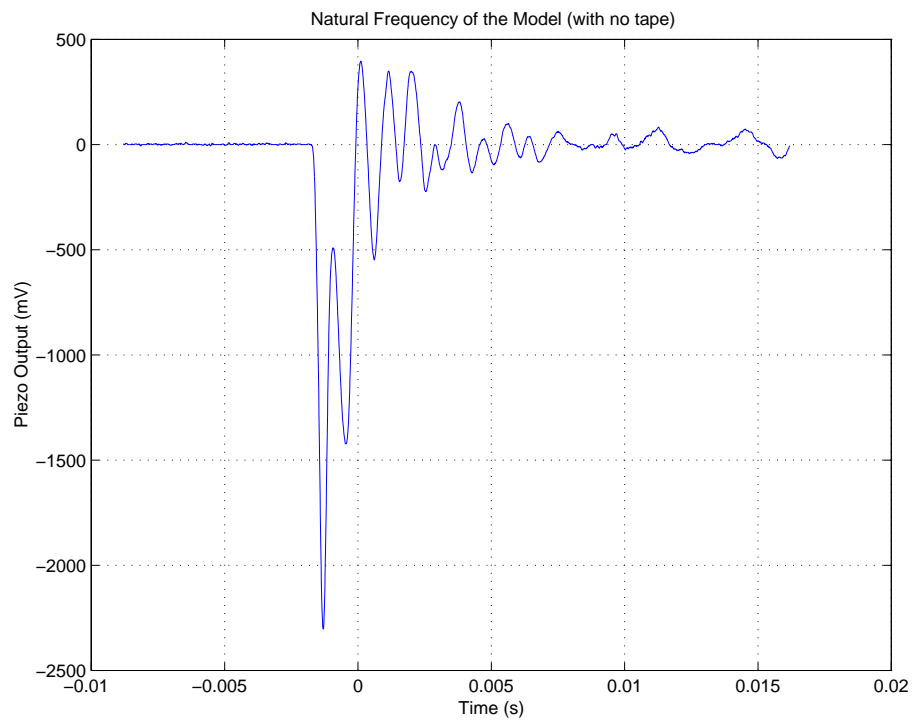


Figure 5.7: The frequency response of the system

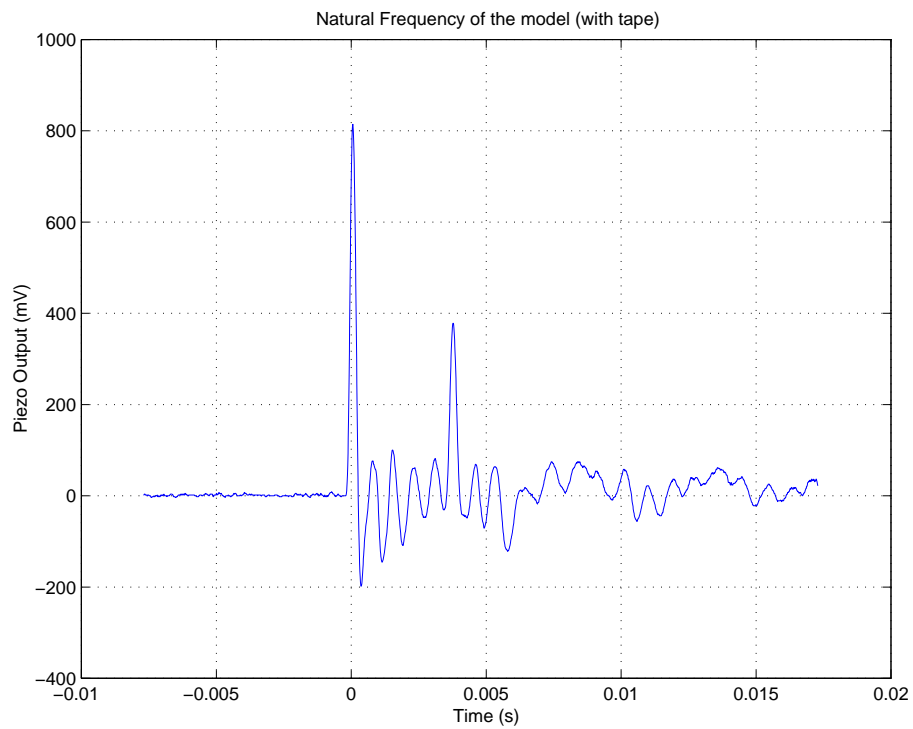


Figure 5.8: The frequency response of the system with tape connection

5.5 Chapter Summary

This chapter has given an overview the new design of the force measurement system and the factors that were taken into consideration when designing this system.

Calculations were also performed to ensure the piezoelectric films would be exposed to strains within their linear operating range.

The performance of this system was tested to ensure it had improved as required. The main improvement was that the natural frequency has increased to approximately 1.1kHz from the original value of 500Hz.

The changes to the USQ Force measurement system include:

- The I-beam was modified to increase the natural frequency
- Additional piezoelectric films were added to allow for the identification of the centre of pressure
- Tape was used to seal the isolate the piezoelectric films (within the protective sleeve) from the flow.

The accuracy of the system was checked through calibration and was seen to be quite good with a variation in the sensitivity of the piezoelectric film of less than 2%.

Chapter 6

Test Run Setup

6.1 Chapter Overview

For the first test run the model will be exposed to the flow at zero angle of attack. Thus only axial forces will be experienced by the model. While this will not assess the systems ability to measure normal forces, it will provide insight into the accuracy of the piezoelectric films in the Gun Tunnel operation. Because of the nature of axial loading, all strain gauges should experience the same strain and therefore should predict the same value of force.

This test will be conducted at lower pressures of approximately 3MPa. This will create smaller forces than a high pressure test run, but will importantly still be operating at Mach 7.

This chapter will give an overview of how the force measurement system will be set up for the first low pressure test run. The settings of electrical equipment will be described. In addition to this, insight will be given into the problems that were experienced while setting up for the test run.

6.2 Measurement Setup

When setting up the force measurement system in the Gun Tunnel the sting was first positioned, then all wires were connected. When this was done, the response of all of the piezoelectric films was checked. Finally the protective sheath was slid into position and the model was screwed onto the end of the cantilever. Again the films were checked again to ensure all were functioning properly.

To assist with the testing procedure, the amplifier and oscilloscope had to be positioned to allow for easy operation. For testing in the USQ Gun Tunnel, the charge amplifier was positioned on top of the dump tank (close to the test section) and was connected to the oscilloscope using coaxial cable. The oscilloscope was positioned near the barrel of the Gun Tunnel, where it could be connected to the computer by serial cable.

For any test run, it is important that all measurement devices are set to record maximum detail for greater accuracy without missing any of the signal.

6.2.1 Oscilloscope

The voltage was be set to 1 Volt per division. This may be a little too large, but will ensure that all of the data is recorded. It must be realised that if the voltage being measured goes outside the set range of the oscilloscope, the missing data cannot be retrieved. Because the number of tests that can be performed is limited, we must ensure that this does not happen.

The oscilloscope will be set to a time scale of 2.5ms per division. This will allow for the measurement of the full 25ms run time.

It is also vital that the oscilloscope is triggered to start recording at exactly the right time. The oscilloscope will be triggered externally by means of the pressure transducer. The oscilloscope must also be set to trigger only once (single trigger) to ensure that the data is not overwritten if it is re-triggered.

6.2.2 Charge amplifier

The charge amplifier was set to produce $\left(\frac{3.16}{3}\right)$ V per nanocoulomb. It has the capacity for four separate channels.

Input to the charge amplifier is through a microdot connection. The output of the amplifier is through BNC plugs, all of which are located on the back of the unit.

The amplifier had the option of battery operation, but was connected through mains power due to problems with the battery.

6.3 Connection of piezoelectric films

In order to connect the piezoelectric films to the conditioning amplifier, the enamel coated wires that were connected to the strain gauge were soldered to BNC plugs located inside the wall of the test section. A connection was then made from these plugs to the amplifier (as can be seen in figure 6.1). This means that the test section remains completely sealed during the test.

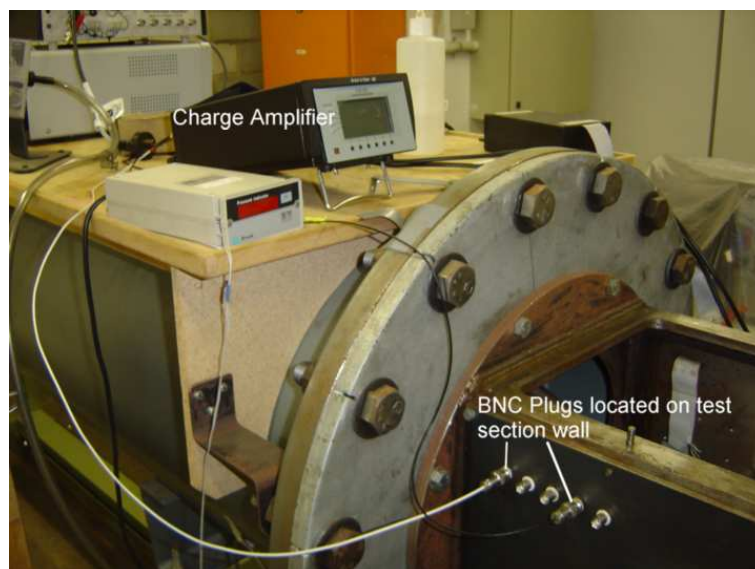


Figure 6.1: Location of BNC connection on test section wall

6.3.1 Protection from Flow Effects

At this stage, it was of concern that the wires exposed inside the test section would be damaged by the flow. The four twisted pairs of wires are completely protected inside the sleeve, but must be connected to the wall of the test section. This means that if not shielded they would be either broken by the flow or exposed to extreme temperatures that could interfere with the results.

A protective bracket was mounted on the wall of the test section and extended to within 5mm of the point where the wires exit the protective sleeve. The wires were then inserted into a small plastic tube and strapped to the bracket. Any loose wires were then taped to the wall. This can be seen in figure 6.2. This bracket should offer acceptable protection for the wires.



Figure 6.2: Wires protected from flow region

6.4 Problems

In setting up the force measurement system, some complications were experienced. When the protective sleeve was being screwed in place, one of the wires was pulled out of position and squashed between the sleeve and the 20mm steel bar. To repair this a new wire would have to be bonded to the film. In addition to this, one of the other

piezoelectric films ceased to work for unknown reasons.

Under normal circumstances, this problem could be fixed in a couple of days, however due to time constraints, the test was performed with only two piezoelectric films working. This is not critical for a test with zero angle of attack.

6.5 Chapter Summary

This chapter has given a detailed description of the setup for the force measurement system in the USQ Gun Tunnel. This included not only the physical setup, but also the settings of the electrical equipment. In addition to this, the aims of the testing have been outlined.

Chapter 7

Results and Discussion

7.1 Chapter Overview

This chapter will present the results of the low pressure test run. These results will be used to calculate the forces on the model. These forces will then be compared to a theoretical prediction based on the measured pressure.

7.2 Flow Quality

The first thing to examine with the test run is the output of the pressure transducer. This will give an indication of the time period where the forces can be measured. Obviously the forces on the model will only simulate atmospheric re-entry when the pressure is relatively steady.

The pressure that was measured can be seen in figure 7.1. In this graph the red line represents the pressure. The region of steady flow was determined by visual inspection and is between the two vertical black lines. Between these lines (in black) is a least squares fit to the pressure data. The average value of this function is the pressure value that will be used for the average pressure calculations.

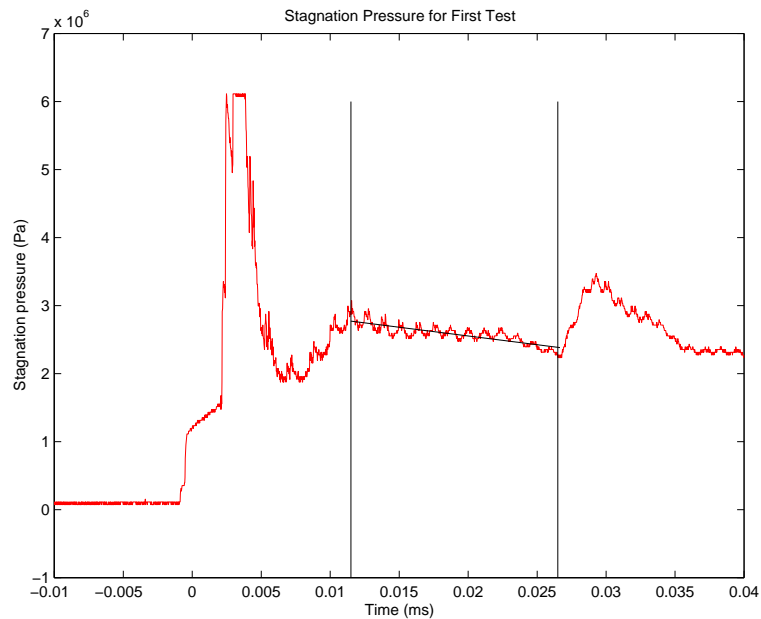


Figure 7.1: Graph showing average pressure during force measurement

The average pressure was **2.58MPa**. The time over which this flow was experienced was from 11.5ms to 26.5 ms. This gives 15ms in which to take force measurements.

7.3 Measured Results

The results for the test run can be seen in figure 7.2.

In order to predict forces on the model, the strain in the period from 11.5ms to 26.5ms must be determined. Therefore an average voltage must be found over this range.

However, due to the setup of the oscilloscope the voltage was not recorded very well. The voltage division was set too large and poor measurements were taken. These results were improved using a matlab script to smooth the values. The corrected strain measurements can be seen in figure 7.3.

On this graph, the values that need to be found are the change in the voltage for each channel. That is, the initial voltage should be compared to the value during steady pressure.

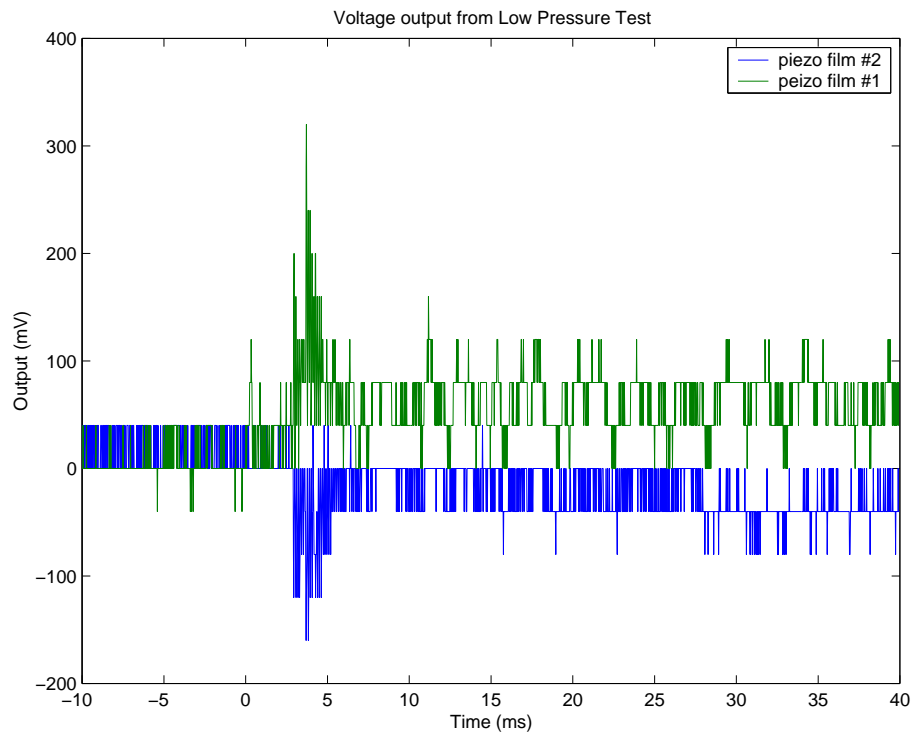


Figure 7.2: Results of strain measurement system for the test run

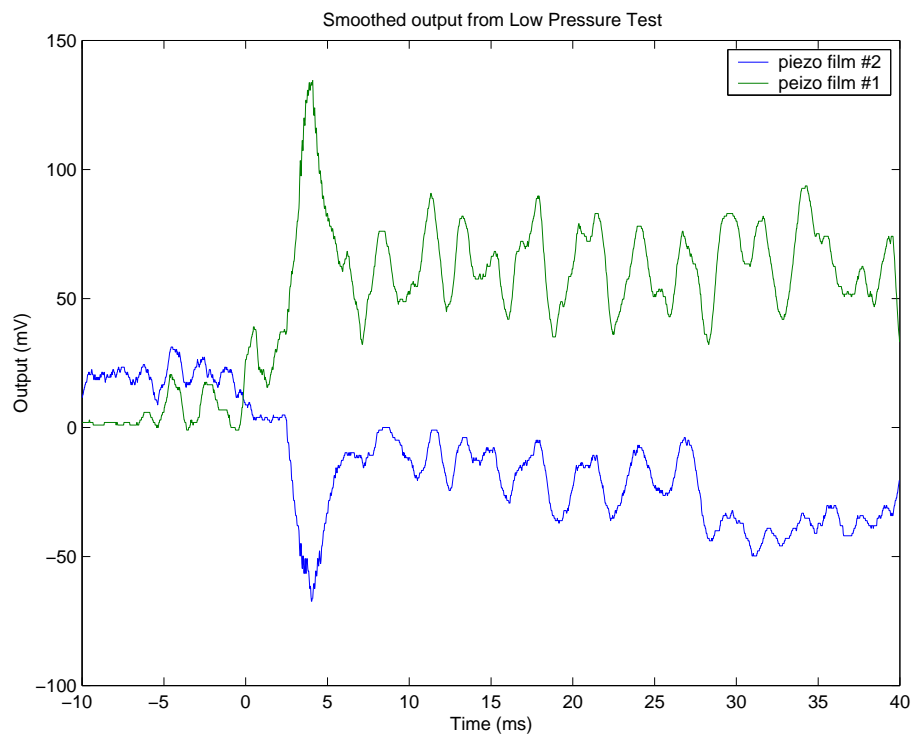


Figure 7.3: Smooth results of test run

The change in voltage for channel one is: 59.83mV

The change in voltage for channel two is: 38.87mV

From examination of the results, the natural frequency was determined to be approximately 500Hz. This is significantly lower than the 1.1kHz that was expected.

7.3.1 Piezoelectric Response

To check the response of the piezoelectric films and ensure that the measurement was triggered at the right time, it would be helpful to plot the strain measurement on the same axis as the pressure printout. Figure 7.4 shows that the films triggered at the right time and even picked up small fluctuations in pressure towards the end of the run. This graph is not drawn to scale and was only used to check the piezoelectric response.

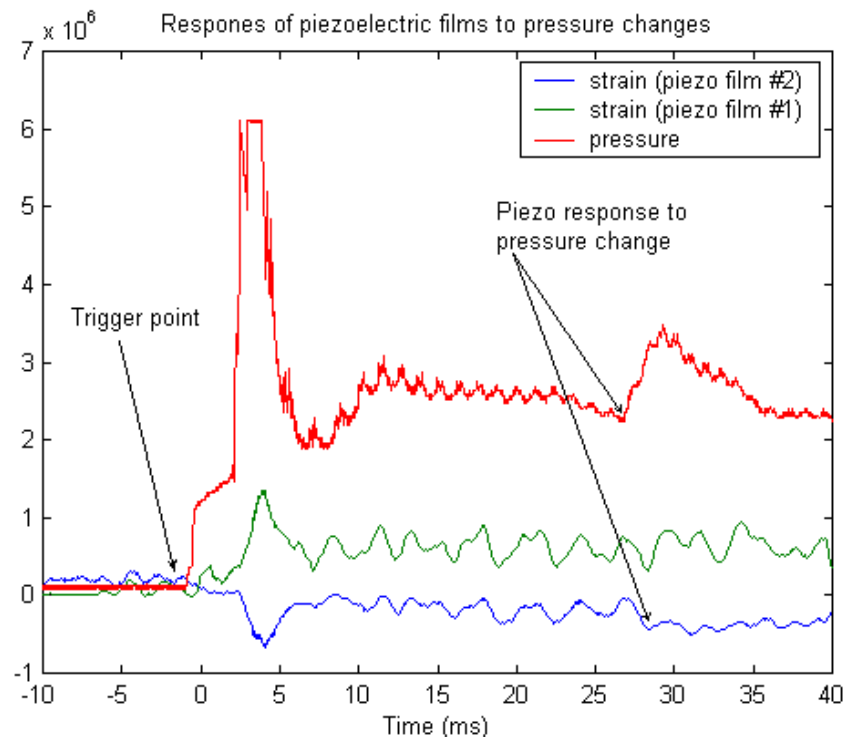


Figure 7.4: Graph of response of piezoelectric films to pressure changes

7.4 Finding the Aerodynamic Force

7.4.1 Calibration

The system was calibrated after the test in the USQ Gun Tunnel, without changing the setup. This means that the calibration will give an accurate indication of the piezoelectric sensitivity during the test run. An example of the measurements recorded during calibration can be seen in figure.

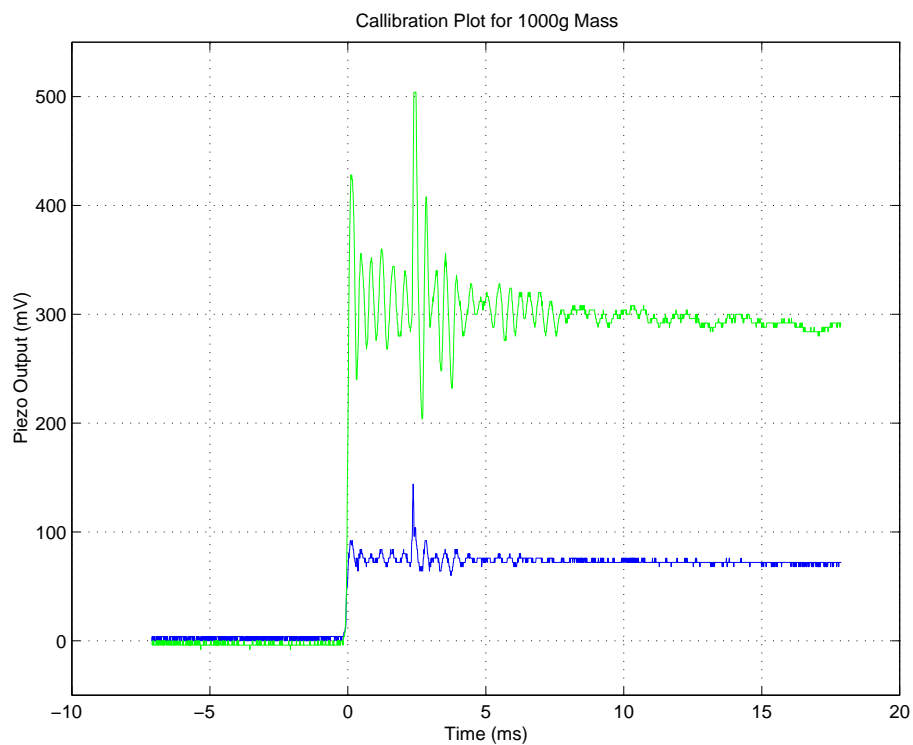


Figure 7.5: Example of calibration data

On this graph, the rapid change in voltage indicates the point where the masses were released. The value that needs to be calculated is the total change in voltage when the masses are cut. By doing this for a number of different masses, the sensitivity of the piezoelectric films can be found quite accurately. A summary of the calibration results can be seen in table 7.1 for the first piezoelectric film and table 7.2 for the second.

This data was then graphed to get the average value of sensitivity. This can be seen in figures 7.6 and 7.7.

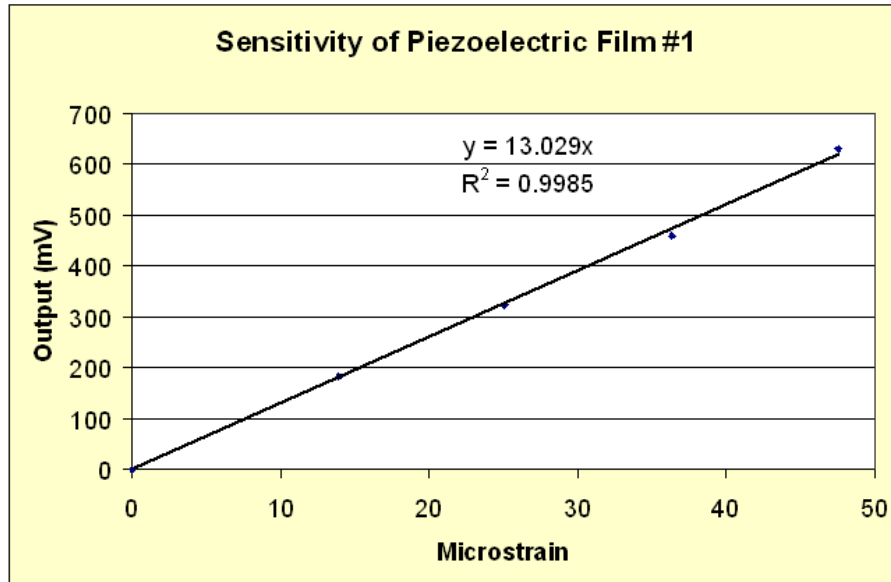


Figure 7.6: Graph used to determine sensitivity of first Piezo film

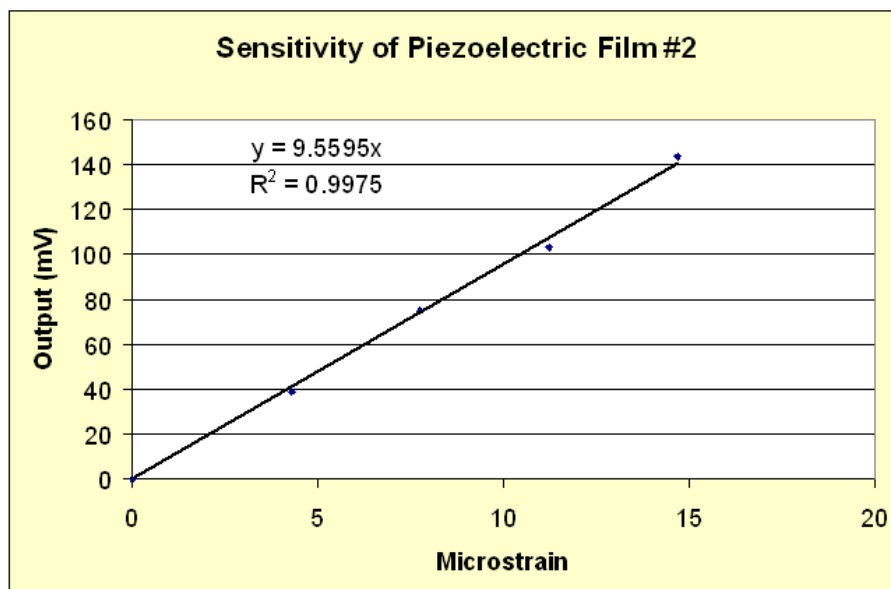


Figure 7.7: Graph used to determine sensitivity of second Piezo film

Hanging Mass (kg)	Expected Strain ($\mu\varepsilon$)	Measured Voltage (mV)	Sensitivity mV/ $\mu\varepsilon$
0.0000	0.000	0.000	na
0.6179	13.874	182.0	13.12
1.1159	25.056	322.7	12.88
1.6179	36.327	459.7	12.65
2.1159	47.509	631.0	13.28

Table 7.1: Data from calibration of no. 1 Piezo film

Hanging Mass (kg)	Expected Strain ($\mu\varepsilon$)	Measured Voltage (mV)	Sensitivity mV/ $\mu\varepsilon$
0.0000	0.000	0.000	na
0.6179	4.2918	38.794	9.04
1.1159	7.7510	75.052	9.68
1.6179	11.239	103.57	9.22
2.1159	14.6971	143.60	9.77

Table 7.2: Data from calibration of no. 2 Piezo film

From this calibration it has been that;

- The sensitivity of piezoelectric film 1 = **13.03** $\frac{mV}{\mu\varepsilon}$
- The sensitivity of piezoelectric film 2 = **9.56** $\frac{mV}{\mu\varepsilon}$

7.4.2 Force Calculation

Using the sensitivities from the calibration, the strain in the cantilever can be calculated. From this strain, the axial force during the test run can be determined. A summary of the calculations can be seen in table 7.3.

Piezoelectric film	Sensitivity (mV/ $\mu\varepsilon$)	Voltage change (mV)	Strain ($\mu\varepsilon$)	Axial Force (mV)
1	9.56	59.83	4.592	20.57
2	13.03	38.87	4.067	18.22

Table 7.3: Forces measured for Low pressure test run

This show that the piezoelectric films predicted forces of **18.22N** and **20.57N**. While

these values should be identical, the difference is quite small and considering all the possible sources of error, are acceptable.

7.5 Expected Results

By modeling the flow with the improved Newtonian flow model, the forces on the model can be predicted. The expected forces were calculated using a stagnation pressure of 2.58 MPa (with equations 2.6 and 2.7) and can be seen in table 7.4. It would be expected that the model experienced forces of 34.3 N in the axial direction and 0 N in the normal direction.

Angle of attack (degrees)	Axial Force (N)	Normal Force (N)
0.0	34.335	0.000
2.5	34.285	0.898
5.0	34.133	1.789
10	33.532	3.532
20	31.211	6.621

Table 7.4: Forces expected for low pressure test run

Based on this information it would appear that there is significant error, either in the force measurement or in the theoretical calculation. A force measurement of 34.3 Newtons was expected when an average value of 19.4 Newtons was measured. This is an error of 43% from the expected value.

It was seen that the natural frequency was significantly lower than was expected and lower than was measured in the test under the same conditions. The frequency that was determined earlier was 1.1kHz compared to the 500Hz that was seen in the low pressure test.

7.5.1 Sources of Error

The error in results indicates that there is an inaccuracy in either in the measurements taken, or the prediction of aerodynamic forces is inaccurate.

The errors that could be associated with force measurement system include;

Inaccurate calibration. The calibration accuracy could be effected by the position at which the force is applied for each test. However this is unlikely to lead to errors of the magnitude that are currently present. It is unlikely that the position at which the force is applied would be out by more than 1 mm. This would not cause an error of 43%.

Errors associated with piezoelectric films. These could include background noise and heating effects. This type of error would probably not lead to errors as significant as those that have been experienced, particularly when the piezoelectric films are well protected.

Poor measurements. The raw data required significant smoothing, this may have given an inaccurate picture of the piezoelectric response. This could account for the discrepancy in the frequencies that were encountered in the test run.

Inaccurate calculations. The calculations based on the Modified Newtonian Flow regime could be inaccurate for this situation. Isentropic flow was assumed throughout the Gun Tunnel. Therefore it is possible that the calculations of the free flow properties of the fluid differ from the actual conditions .

It is extremely unlikely that the temperature effects of the flow could have influenced the results as the piezoelectric films were completely sealed from the external environment.

An important fact in determining the source of error is that both of the piezoelectric films predicted very similar forces. It is therefore possible that the measured value is correct and the theoretical predictions are inaccurate. However, more testing and CFD analysis would be required to substantiate this.

Further investigation would require that more testing be completed, particularly at different angles of attack. This would enable better conclusions to be drawn about the performance of the system and the identification of sources of error. Ideally, computational fluid dynamics (CFD) should be used to analyse the behaviour of the model in

a Mach 7 flowfield. This would give some indication of whether the theoretical model of the forces on the re-entry capsule is correct.

7.6 Chapter Summary

This chapter gave a summary of the results of the first low pressure test run with the improved force measurement system. Results from the testing and subsequent calibration of the system indicated that the forces acting on the model were quite different from what was expected.

From the results, the reasons for the discrepancy could not be identified. It is possible though that the theoretical prediction could be inaccurate.

Chapter 8

Conclusions and Further Work

The majority of the objectives for this project were met, however due to time constraints a full testing program was not completed. Because of this, the effectiveness of the improvement of the force measurement system could not be fully determined.

8.1 Achievement of Project Objectives

The following objectives have been addressed:

Review the work done by a previous 4th year project student. The project work from 2001, of project student Justin Terhorst, was reviewed in chapter 4. This gave insight into the workings of the USQ force measurement system. The results of this system were analysed to find the areas that needed improvement.

Review other aerodynamic force measurement techniques. Other aerodynamic force measurement systems were reviewed to establish the problems that are associated with measuring forces in short duration hypersonic test facilities. This gave guidelines of how to improve the accuracy of force measurement systems.

Perform experiments on existing balance to characterise its dynamics. Experiments were performed on the existing system to establish how the behaviour of the system could be improved. Chapter 4 describes the bench testing that was performed

to determine how the natural frequency and damping of the system were affected by certain modifications.

Develop an engineering model for the dynamics of the (proposed) technique.

The dynamic behaviour of the proposed system was modelled in chapter 5. The natural frequency was predicted and checks were made to ensure the piezoelectric films would operate within normal operating range under all conditions.

Design an improved system. After all background information was considered, the improved system was designed. This was manufactured in the USQ workshop.

Bench test the new system for dynamic characteristics. The new system was bench tested outside of the gun tunnel to see if it had improved as expected. The graphs of these initial tests can be seen in chapter 5 and show a marked increase in natural frequency.

Obtain experimental data on the new system when operated in the gun tunnel.

After the initial testing indicated the improved system would function correctly, a single low pressure test was conducted.

Analyse results and compare with analytical predictions for different body shapes.

The results were analysed and the predicted forces were compared to theoretical calculations. Unfortunately there was discrepancy in these results. Different body shapes were not tested due to a lack of time, however the system could easily support large models that carry greater aerodynamic forces without any changes.

8.2 Further Work

The first thing that would be required of anyone continuing this project, would be to conduct further Gun Tunnel tests with all four piezoelectric strain gauges working. These tests should be at an angle of attack greater than zero to test the system's ability to measure normal forces as well as axial forces.

Another valuable exercise would be to simulate the flow across the re-entry capsule using

Computational Fluid Dynamics (CFD). If the forces on the model could be estimated with CFD, the results could then be compared to the experimental and analytical values to give a better idea of the system performance.

It would also be beneficial to develop a method of application for piezoelectric films, that could help to reduce noise levels and the effects of external power sources.

Even though little testing has taken place on the improved force measurement system, it is expected that forces will be measured reasonably accurately in both normal and axial directions.

References

- Allgre, J. (1997), ‘Aerodynamic forces and moments for a re-entry module’, *Spacecraft and Rockets* **34**(2), 182–185.
- Balachandran, B. (2004), *Vibrations*, Bill Stenquist, Belmont, USA.
- Bertin, J. J. (1994), *Hypersonic Aerothermodynamics*, AIAA Education Series, American Institute of Aeronautics and Astronautics, Inc., Washington, DC.
- Duncan, W. J. (1974), *Mechanics of Fluids*, second edn, Edward Arnold, Port Melbourne, Australia, pp. 459–496.
- Fox, R. W. (1998), *Introduction to Fluid Mechanics*, fifth edn, John Wiley & sons, New York.
- John D. Anderson, J. (1989), *Hypersonic and High Temperature Gas Dynamics*, Aeronautical and Aerospace Engineering, McGraw-Hill, Boston, Massachusetts.
- Mee, D. (2003), ‘Dynamic calibration of force balances for impulse hypersonic facilities’, *Shock Waves* **12**, 443–455.
- Smith, A. L. (n.d.), The application and performance of piezoelectric film as a dynamic strain sensor, Technical report, University of Queensland.
- Störkmann, V. (1998), ‘Force measurements in hypersonic impulse facilities’, *AIAA* **36**(3), 342–348.
- Terhorst, J. P. (2001), Aerodynamic force measurement system for the usq gun tunnel, Beng dissertation, University of Southern Queensland.

W.T.Thomson (1888), *Theory of Vibratoin with Applications*, third edn, Allen & Unwin, London.

Appendix A

Project Specification

The project specification is *always* Appendix A. It will be inserted on the following page when you collate the final document.

University of Southern Queensland
FACULTY OF ENGINEERING AND SURVEYING
ENG 4111/4112 Research Project
PROJECT SPECIFICATION

FOR: **TIMOTHY DAVIDSON**

TOPIC : MEASUREMENT OF ENTRY CAPSULE AERODYNAMIC COEFFICIENTS

SUPERVISOR: Dr. David Buttsworth
A Sharifian


ENROLMENT: ENG 4111 –S1 2004
ENG 4112 –S2 2004

PROJECT AIM: The aim of this project is to extend the existing technique of measuring aerodynamic forces on a re-entry vehicle, so that both the normal and axial forces can be identified as well as the location of the centre of pressure.

PROGRAMME: Issue A, 26th March 2004

1. Review the work done by a previous 4th year project student.
2. Review other aerodynamic force measurement techniques.
3. Perform experiments on existing balance to characterise its dynamics.
4. Develop an engineering model for the dynamics of the (proposed) technique.
5. Design an improved system.
6. Bench test the new system for dynamic characteristics.
7. Obtain experimental data on the new system when operated in the gun tunnel.
8. Analyse results and compare with analytical predictions for different body shapes.

AGREED:

 (Student) _____ (Supervisors)
28/10/04 _/ _/ _/ _/

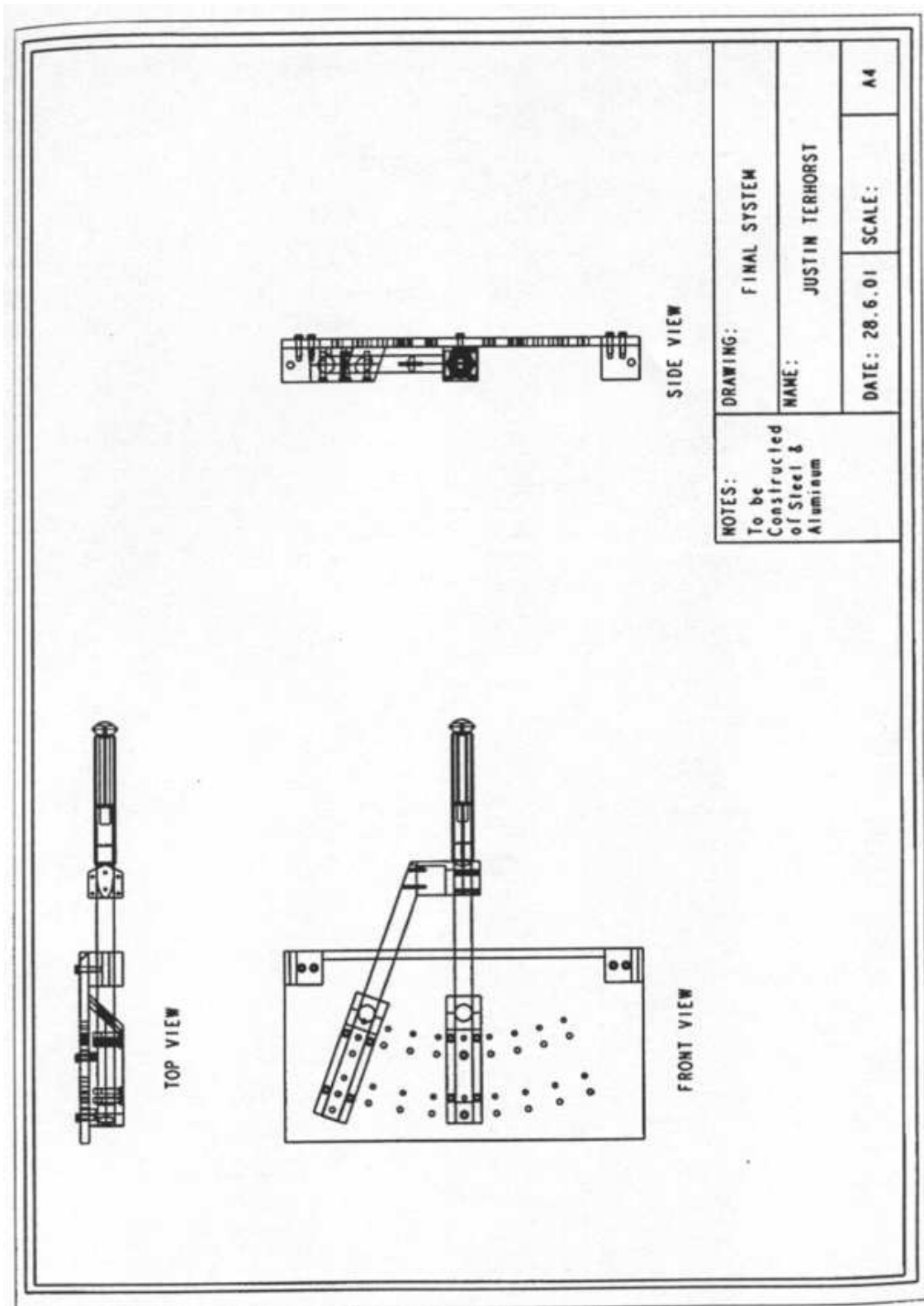
Appendix B

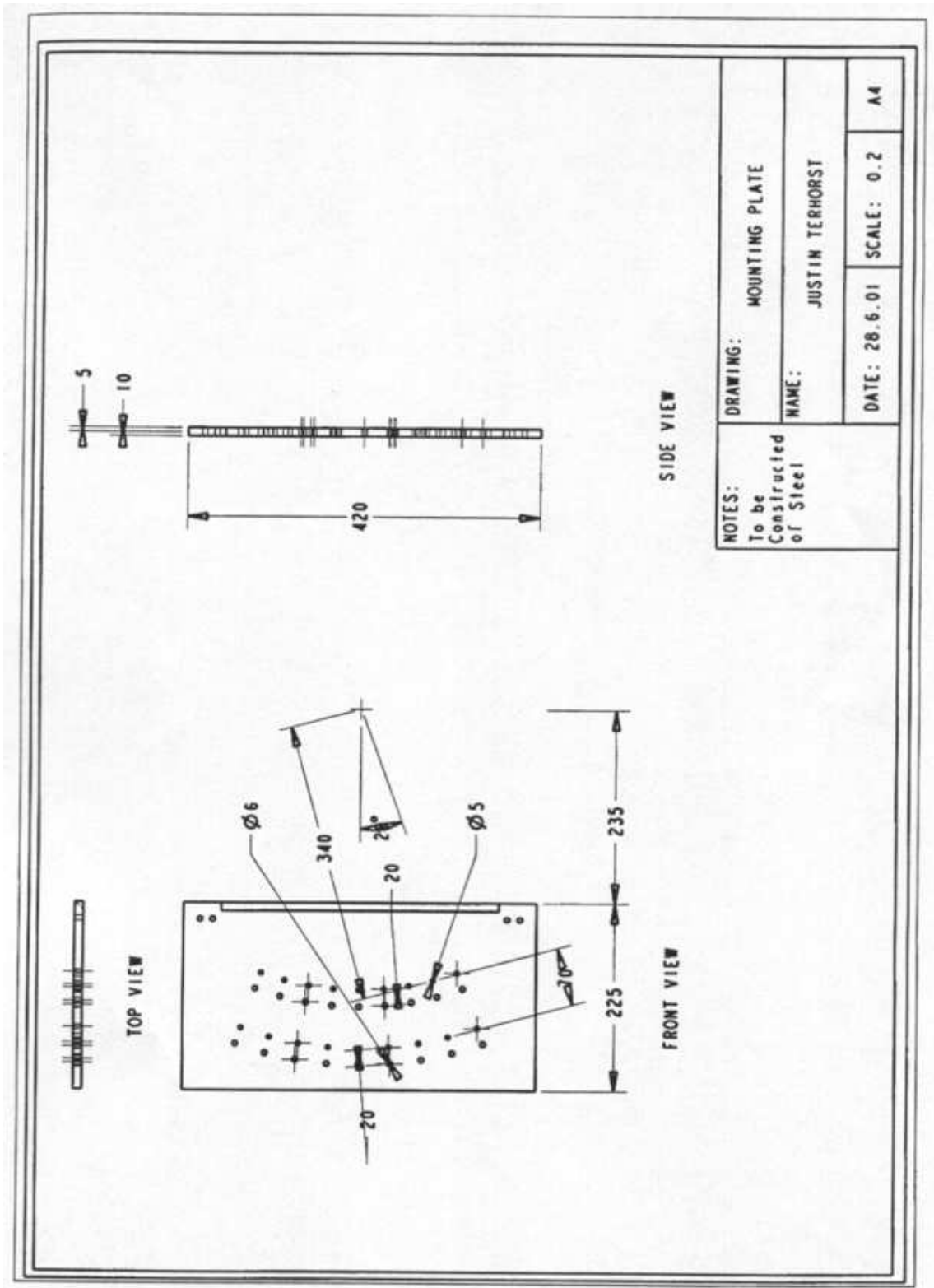
System Drawings

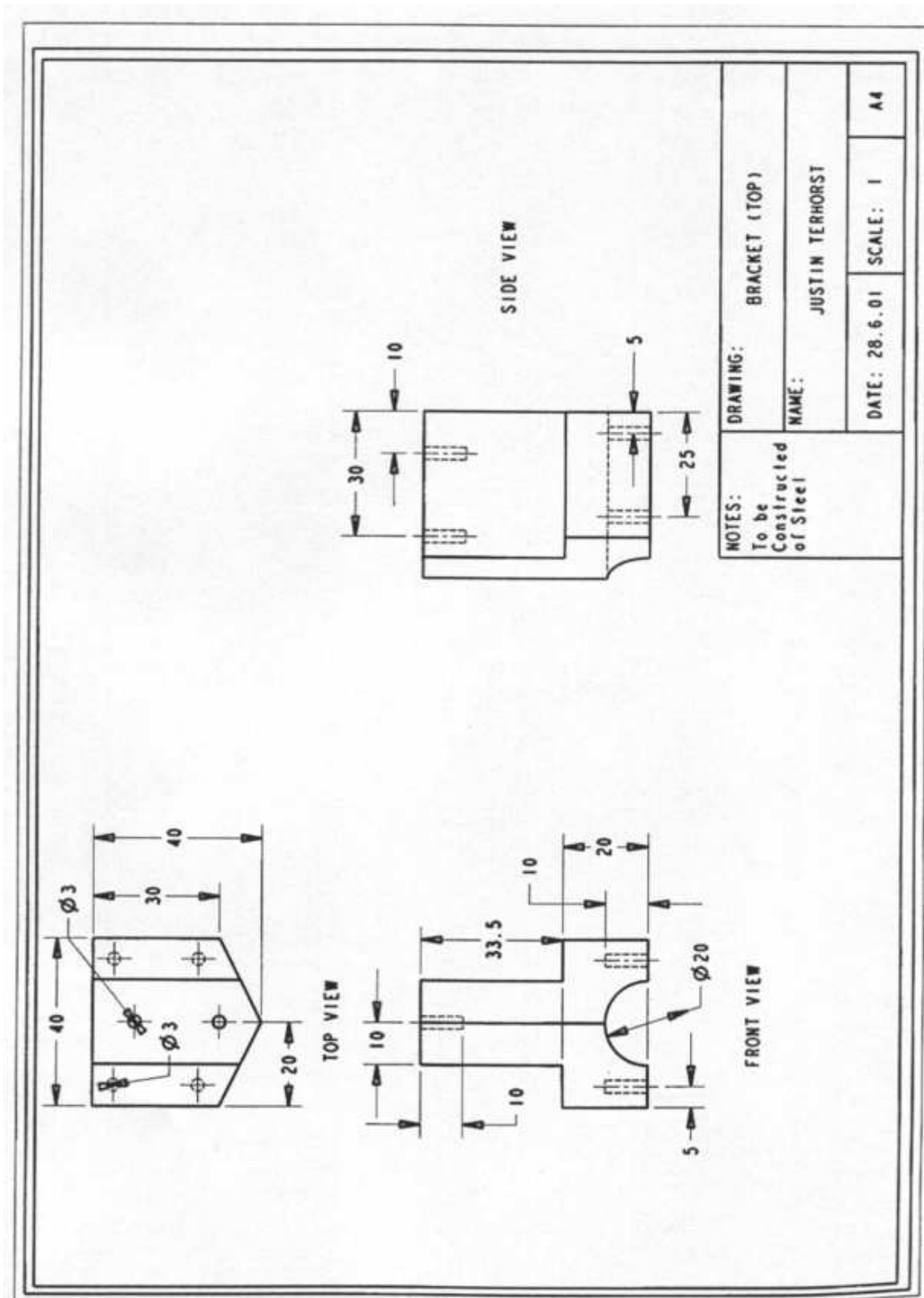
This Appendix will contain Drawings of the existing force measurement system as well as modified components

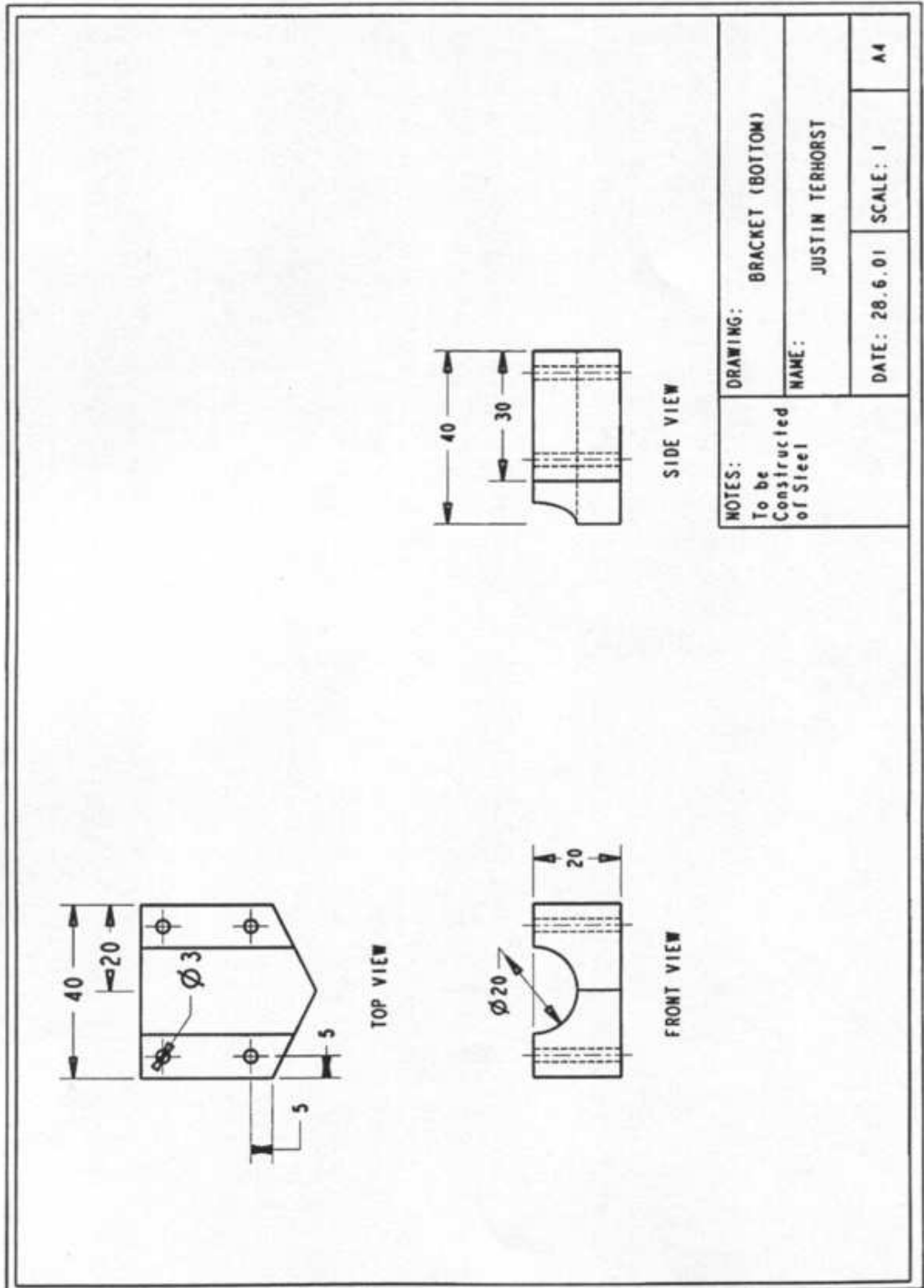
B.1 Original Drawings

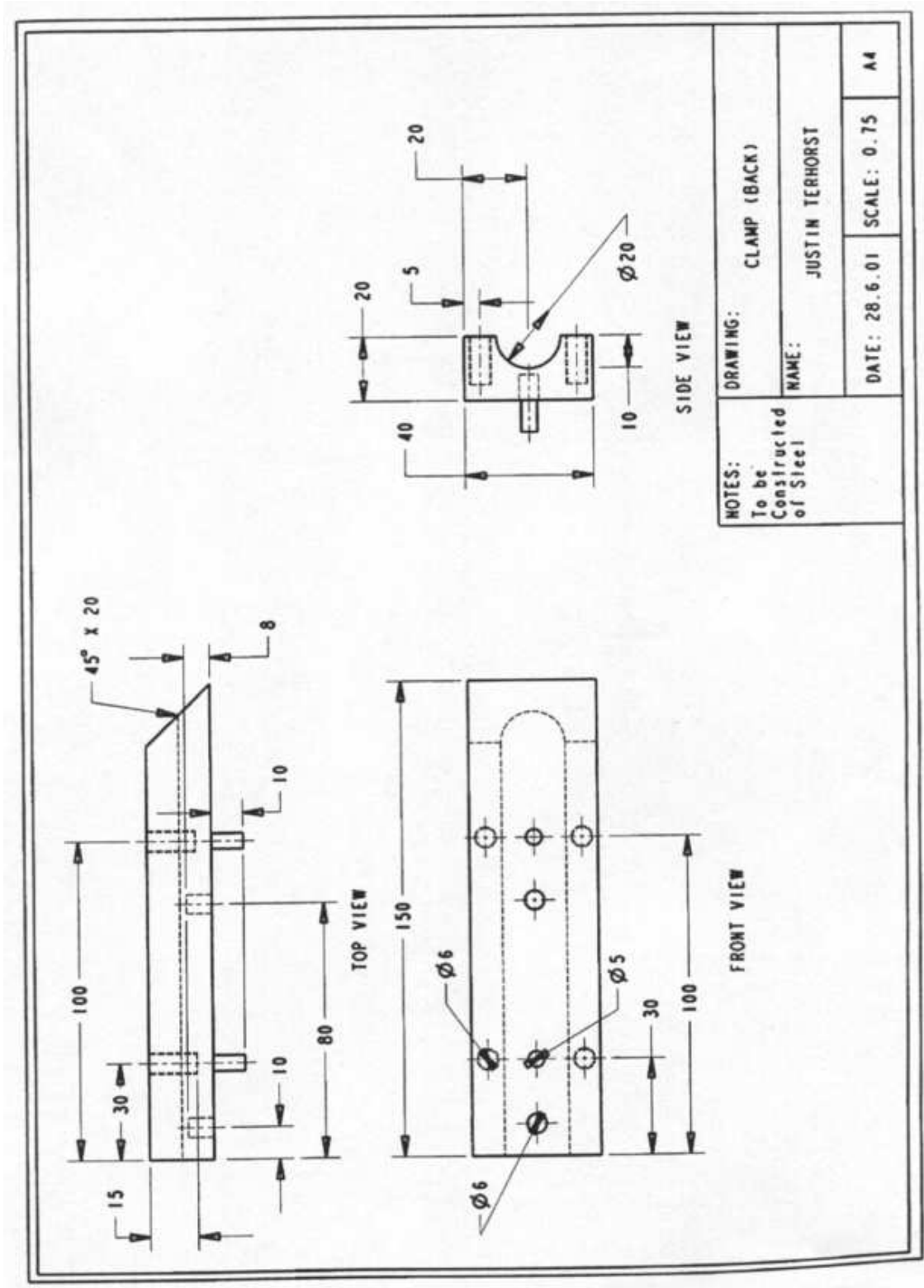
All original Drawings are from Terhorst (2001).

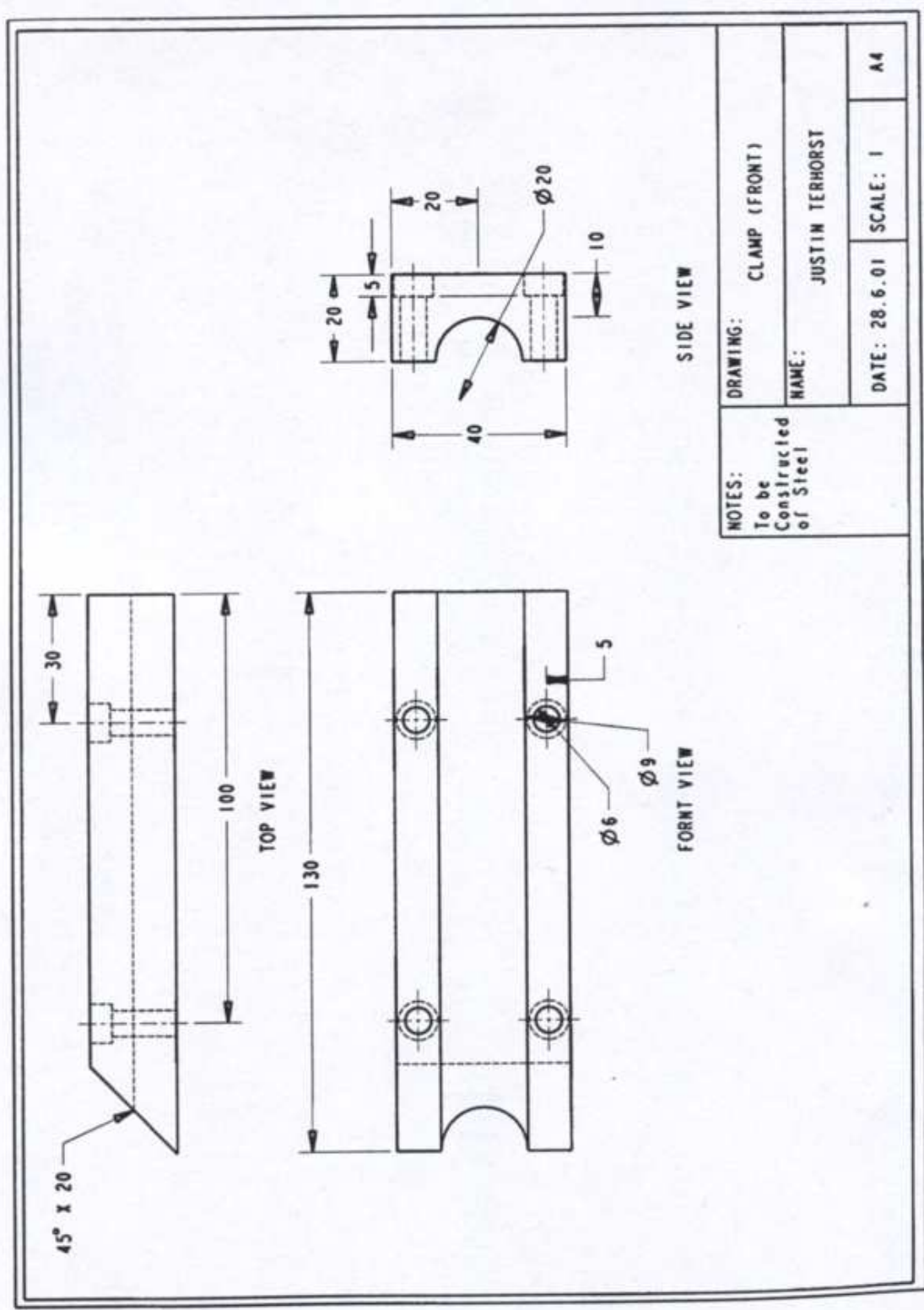


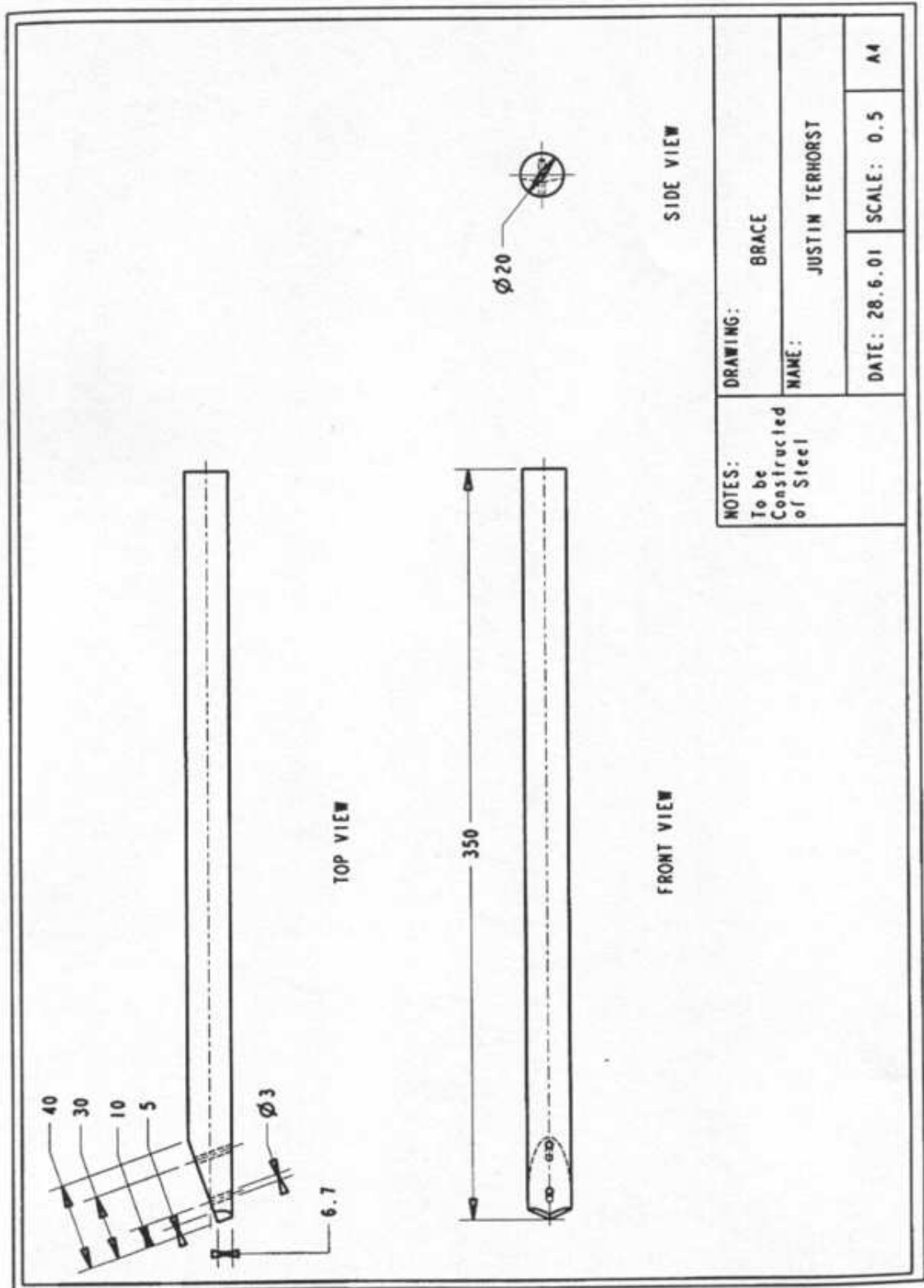


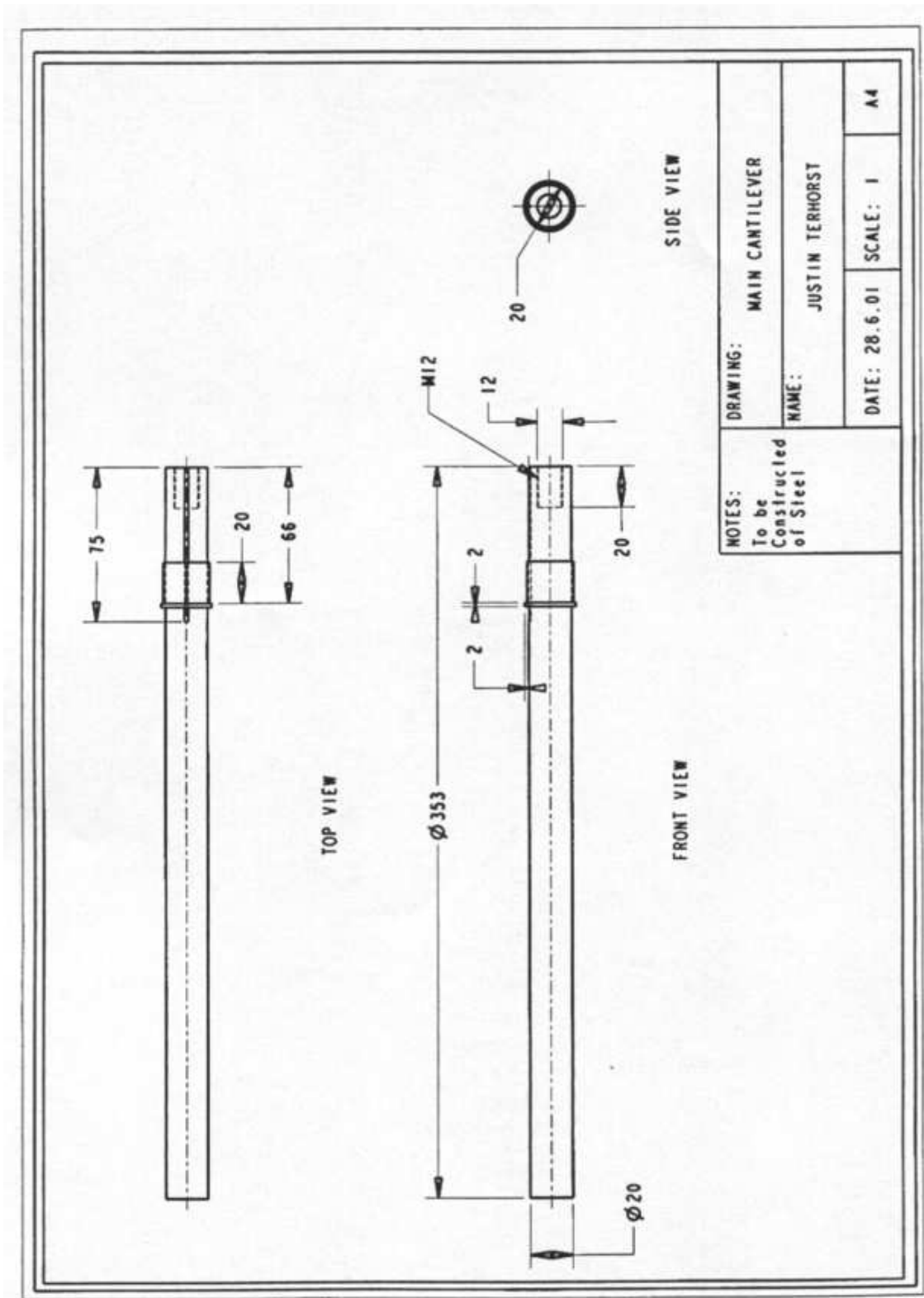


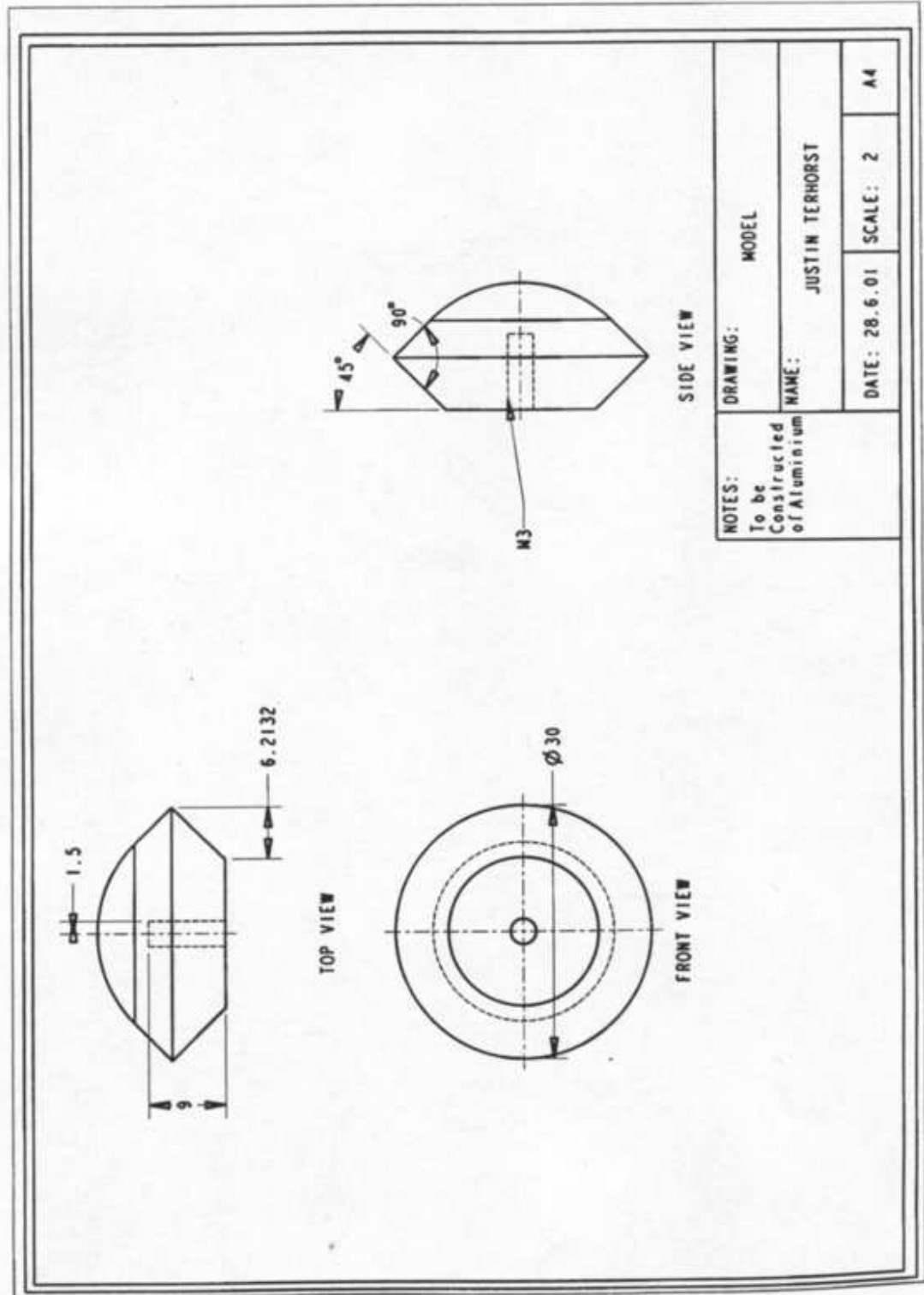


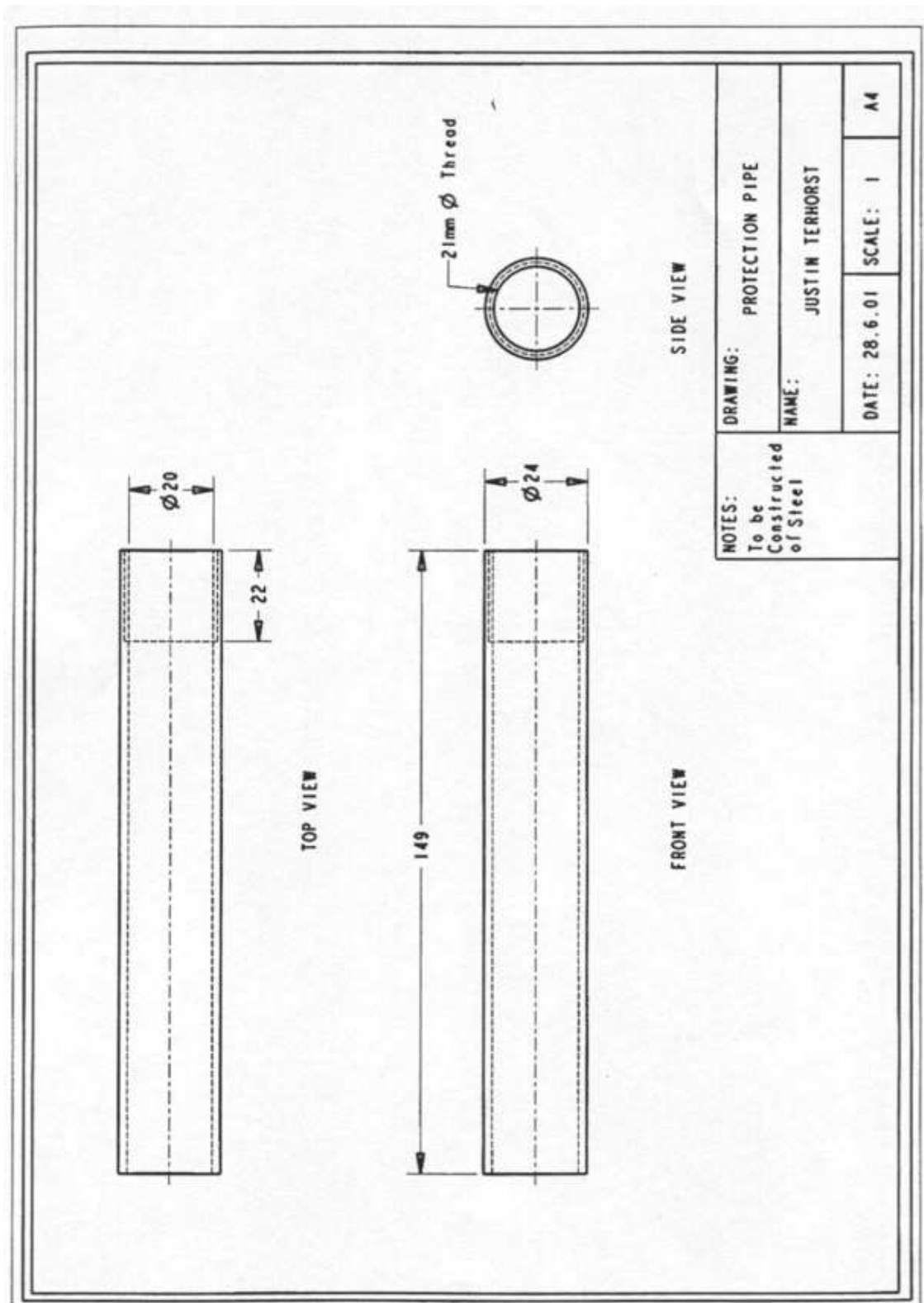












B.2 Improved component

This is the modified I-Beam.

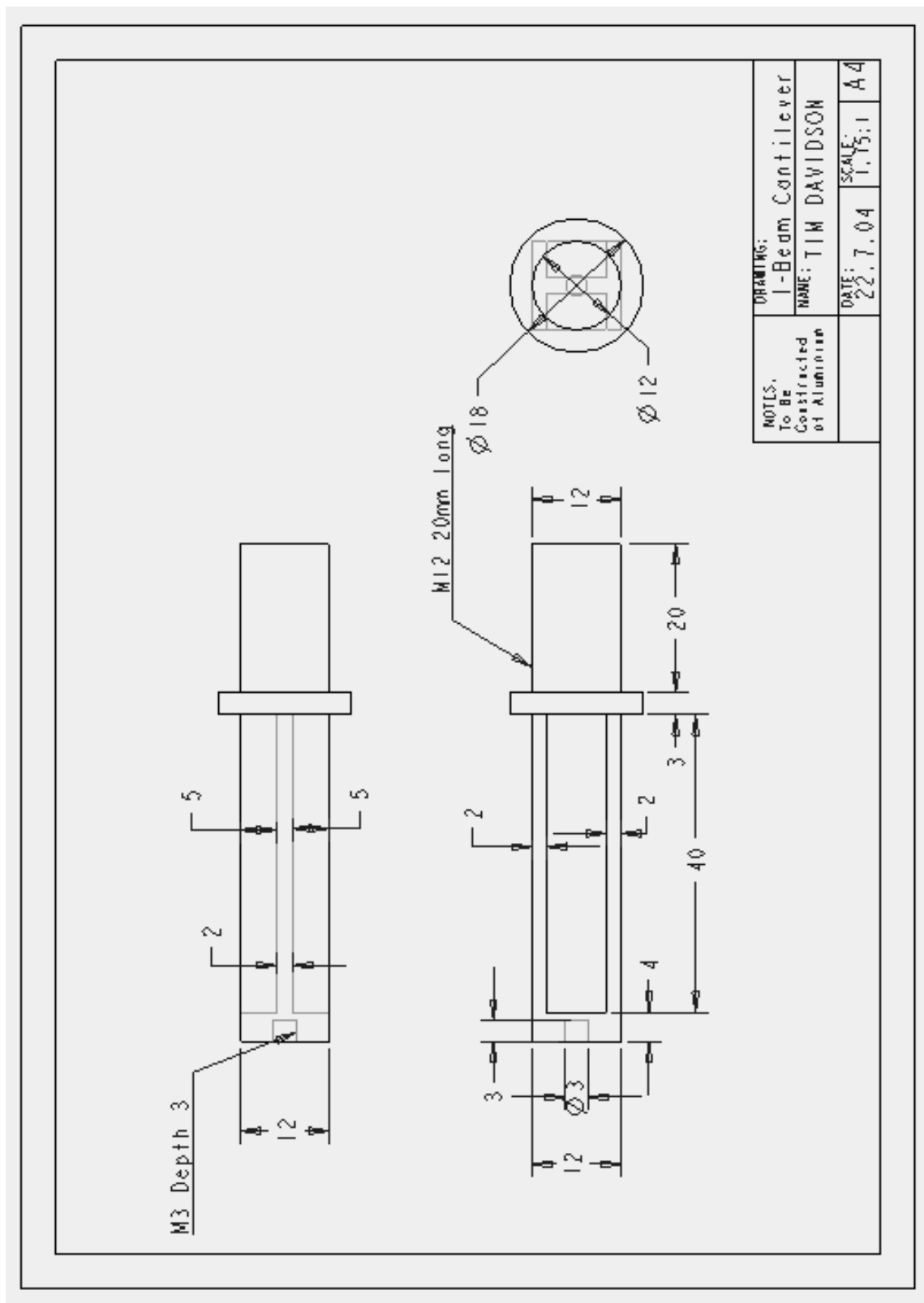


Figure B.1: The new I-beam cantilever

Appendix C

Calculations

C.1 Force Prediction

Calculation of Axial and Normal forces for the low pressure test run.

First the stagnation point pressure coefficient must be found

Stagnation Point Pressure Coefficient, $C_{pt2} = 1.82$

It is known for this example that $M = 7.0$

and $\gamma = 1.4$ for air,

$$\begin{aligned}\frac{p_{t2}}{p_1} &= \left[\frac{(\gamma+1)M_1^2}{2} \right]^{\frac{\gamma}{\gamma-1}} \left[\frac{\gamma+1}{2\gamma M_1^2 - (\gamma-1)} \right]^{\frac{1}{\gamma-1}} \\ &= 63.5526\end{aligned}$$

The stagnation point pressure coefficient was then found;

$$\begin{aligned}C_{pt2} &= \left[\frac{p_{t2}}{p_1} - 1 \right] \frac{2}{\gamma M_1^2} \\ &= 1.82\end{aligned}$$

For the calculation of the Force coefficients, the known values are:

Stagnation Point

Pressure Coefficient, $C_{pt2} = 1.82$

Nose radius, $R_N = 0.015m$

Base radius, $R_B = 0.015m$

Cone angle, $\theta_c = 45^\circ = 0.7854rad$

Angle of attack, α , will vary from -20 to +20 degrees.

The Axial force coefficient can be found by substituting the given values into the equation below.

$$C_A = 2C_{pt2} \left(\frac{R_N}{R_B} \right)^2 \left[\begin{aligned} &(0.25 \cos^2 \alpha (1 - \sin^4 \theta_c) + 0.125 \sin^2 \alpha \cos^4 \theta_c) + \\ &\tan \theta_c (\cos^2 \alpha \sin^2 \theta_c + 0.50 \sin^2 \alpha \cos^2 \theta_c) \times \\ &\left(\frac{(R_B/R_N) - \cos \theta_c}{\tan \theta_c} \cos \theta_c + \frac{((R_B/R_N) - \cos \theta_c)^2}{2 \tan \theta_c} \right) \end{aligned} \right] \quad (C.1)$$

The normal Force can be found by substituting the given forces into the equation below.

$$C_N = 2C_{p,t2} \left(\frac{R_N}{R_B} \right)^2 \left[0.25 \sin \alpha \cos \alpha \cos^4 \theta_c + \sin \alpha \cos \alpha \sin \theta_c \cos \theta_c \times \left(\frac{(R_B/R_N) - \cos \theta_c}{\tan \theta_c} \cos \theta_c + \frac{((R_B/R_N) - \cos \theta_c)^2}{2 \tan \theta_c} \right) \right] \quad (C.2)$$

The values for the force coefficients can be seen in the table below. Only angles of attack of 0 to 20 degrees have been looked at, as the force coefficient of $\alpha = -20^\circ$ would simply be the negative of $\alpha = +20^\circ$.

Angle of attack (degrees)	Axial Force Coefficient	Normal Force Coefficient
0.0	1.1375	0.0000
2.5	1.1358	0.0297
5.0	1.1308	0.0593
10	1.1109	0.1167
20	1.0340	0.2194

To find the forces the density and velocity in the free stream must be determined. It has been assumed that the flow that takes place in the Gun Tunnel is isentropic.

Must first find density at stagnation conditions;

$$T_o = 750K$$

$$R_{air} = 287$$

$$P_o = 2.58MPa$$

(from pressure transducer measurement)

$$\begin{aligned} \rho_o &= \frac{P_o}{RT_o} \\ &= \frac{2.58 \times 10^6}{287 \times 750} \\ &= 11.986kg/m^3 \end{aligned}$$

assuming isentropic change,

$$\frac{\rho_0}{\rho_1} = 383.32$$

$$\rho_1 = 0.031233 \text{ kg/m}^3$$

and

$$\frac{T_0}{T_1} = 10.8$$

$$T_1 = 69.44 \text{ K}$$

To find the free stream velocity now,

$$\begin{aligned} U_1 &= M \times \sqrt{RT_1\gamma} \\ &= 7 \times \sqrt{287 \times 69.44 \times 1.4} \\ &= 1169.29 \text{ m/s} \end{aligned}$$

Now the Forces can be determined from using the free stream values just found

$$F_N = C_N \rho_1 U_1^2 \Pi R_B^2 \quad (\text{C.3})$$

$$F_A = C_A \rho_1 U_1^2 \Pi R_B^2 \quad (\text{C.4})$$

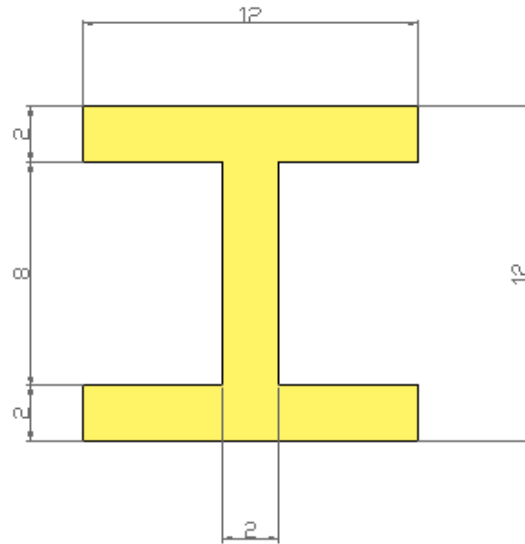
The table of calculated forces can be seen below.

Angle of attack (degrees)	Axial Force (N)	Normal Force (N)
0.0	34.335	0.000
2.5	34.285	0.898
5.0	34.133	1.789
10	33.532	3.532
20	31.211	6.621

C.2 frequency prediction calculations

This will show how the natural frequency of the cantilever was estimated.

First though, the section properties of the cantilever must be found. The cross section of the I-beam cantilever can be seen below.



Cross-section of I-Beam

Figure C.1: Cross section of the I-Beam cantilever

The second moment of Inertia , I

For a rectangle, $I_{xx} = \frac{bh^3}{12}$

where $b = \text{breadth}$ and $h = \text{height}$

For an I-beam of this size,

$$\begin{aligned} I &= \frac{12 \times 12^3}{12} - \frac{10 \times 8^3}{12} \\ &= 1.013 \times 10^{-9} m^4 \\ &= 1301.33 mm^4 \end{aligned}$$

Now that this is known, we can model the model and sting as a mass on a uniformly loaded beam. This can be seen in figure 5.5.

The values important to this system are.

$$\begin{aligned}
\text{Mass of model, } M &= 0.016 \text{ kg} \\
E_{\text{aluminium}} &= 7 \times 10^{10} \text{ Pa} \\
\text{Length of Cantilever, } l &= 0.047 \text{ m} \\
\text{Cross – sectional area, } A_{cs} &= 6.4 \times 10^{-5} \text{ m}^2 \\
\text{Density of Aluminium, } \rho_{al} &= 2710 \text{ kg/m}^3
\end{aligned}$$

Therefore the mass of the cantilever is,

$$m_c = 0.08152 \text{ kg}$$

The frequency of the cantilever, w_{11} is

$$\begin{aligned}
\omega_{11}^2 &= 3.515^2 \left(\frac{EI}{ml^3} \right) \\
&= 3.515^2 \left(\frac{7 \times 10^{10} \times 1.013 \times 10^{-9}}{0.08152 \times 0.047^3} \right) \\
&= 1.329797 \times 10^{+9}
\end{aligned}$$

The frequency of the model, w_{22} is;

$$\begin{aligned}
\omega_{22}^2 &= 3.00 \left(\frac{EI}{Ml^3} \right) \\
&= 3.00 \left(\frac{7 \times 10^{10} \times 1.013 \times 10^{-9}}{0.016 \times 0.047^3} \right) \\
&= 1.645065 \times 10^{+8}
\end{aligned}$$

These can then be combined

$$\begin{aligned}
\omega_1^2 &= \frac{\omega_{11}^2 \omega_{22}^2}{\omega_{11}^2 + \omega_{22}^2} \\
&= \frac{(1.329797 \times 10^{+9})^2 \times (1.645065 \times 10^{+8})^2}{(1.329797 \times 10^{+9})^2 + (1.645065 \times 10^{+8})^2} \\
&= 1.4640 \times 10^{+8} \\
\omega_1 &= 12099.4283 \text{ rad/s} \\
&= 1925.7 \text{ Hz}
\end{aligned}$$

The Natural frequency of the Cantilever mass system was estimated to be **1925.7Hz**.

C.3 Calibration

This will outline the calibration process by which the sensitivity of the piezoelectric films was estimated.

The system was calibrated by applying known masses to the end of the cantilever. A schematic diagram of this can be seen in the figure below. In this figure, the location of the centres of the piezoelectric films are represented by yellow dots.

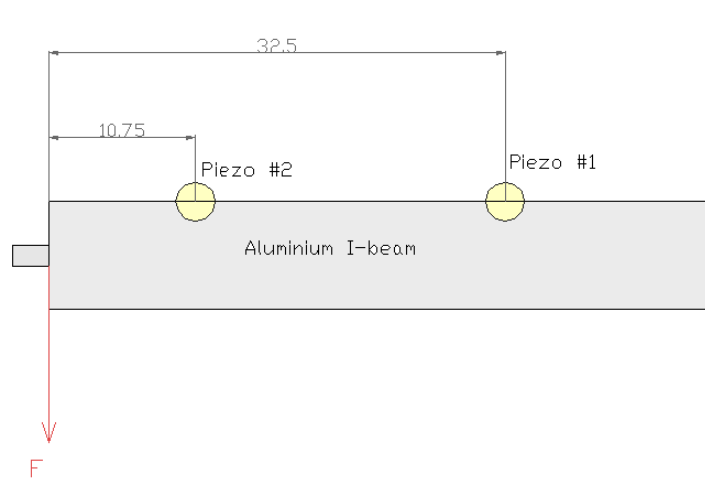


Figure C.2: Diagram of calibration setup

The masses that were applied and their corresponding forces are;

Mass (kg)	Force (N)
0.0000	0.000
0.6179	6.061
1.1159	10.95
1.6179	15.87
2.1159	20.76

The 1.1159kg mass will be used as an example of how to determine the strain in the cantilever.

Will first examine piezoelectric film #1.

It can be seen from the figure that the distance from the line of action of the force to the piezo film is 34.75mm.

$$d_1 = 34.75mm$$

$$F = 10.95 \text{ N}$$

The bending moment at the centre of piezo 1 is;

$$\begin{aligned} M &= F \times d_1 \\ &= 10.95 \times 34.75mm \\ &= 380.40 \text{ Nmm} \end{aligned}$$

The bending moment can then be used to find the stress at the piezoelectric film.

$$\begin{aligned} \sigma &= \frac{M \times y}{I} \\ &= \frac{380.4 \times 6}{1301.33} \\ &= 1.7538 \text{ MPa} \end{aligned}$$

For Aluminium, $E = 7 \times 10^4 \text{ MPa}$

The relationship between modulus of elasticity (E), stress and strain is;

$$\begin{aligned} E &= \frac{\sigma}{\varepsilon} \\ \varepsilon &= \frac{\sigma}{E} \\ &= \frac{1.7538}{7 \times 10^4} \\ &= 2.506 \times 10^{-5} = 25.06 \times 10^{-6} \\ &= 25.06 \mu\varepsilon \end{aligned}$$

Using the piezoelectric properties of the film which were described in chapter ref{chap:improvement} we can calculate the expected output charge.

Known values: Area of film, $A_f = 2 \times 10^{-4}$

Piezoelectric strain constant, $C = 69 \times 10^{-3}$

Strain = 25.06×10^{-6}

$$\begin{aligned}
 \text{Charge, } Q &= 25.06E^{-6} \times 2 \times 10^{-4} \times 69 \times 10^{-3} \\
 &= 3.458 \times 10^{-10} \text{ Coulombs} \\
 &= 0.0138 \text{ nC}
 \end{aligned}$$

Assuming the amplifier output is $(3.16/3.00)V/nC$, this would produce a voltage of 364.24 mV.

The measured value was **322.7 mv** (which was not far from expected). This is of no significance to the calibration but indicates everything is on the right track.

Based on these measurements the sensitivity of the piezoelectric film would be;

$$\begin{aligned}
 \text{Sensitivity} &= \frac{mV}{\mu\varepsilon} \\
 &= \frac{322.7}{25.06} \\
 &= 12.88 \frac{mV}{\mu\varepsilon}
 \end{aligned}$$

This process must be repeated for all of the different masses and both piezoelectric films. The results of the calibration are summarised in the body of the report.

The sensitivity of piezoelectric film 1 is $13.03 \text{ mV}/\mu\varepsilon$.

The sensitivity of piezoelectric film 2 is $9.56 \text{ mV}/\mu\varepsilon$

C.4 Calculating the Aerodynamic Force from Measured Strains

This show the process that was used to calculate the axial forces on the model.

We know that the cross sectional area of the I-beam is $64mm^2$

For piezo 1 a voltage change of 59.83mV was recorded during the test run.

therefore the strain is;

$$\begin{aligned}
 \varepsilon_1 &= \text{measured voltage/sensitivity}_1 \\
 &= 59.83/13.01 \\
 &= 4.592\mu\varepsilon
 \end{aligned}$$

and,

$$\begin{aligned}
 E &= \sigma_1/\varepsilon_1 \\
 \sigma_1 &= E\varepsilon_1 \\
 &= 7 \times 10^4 MPa 4.593 \times 10^{-6} \\
 &= 0.3212 MPa
 \end{aligned}$$

To find the Force from this stress,

$$\begin{aligned}
 F_{A1} &= \sigma_1 \times \text{Area} \\
 &= 0.3212 \times 64.00 \\
 &= 20.57N
 \end{aligned}$$

For piezo 2, a voltage change of 38.87mV was recorded during the test run.

therefore the strain is;

$$\begin{aligned}
 \varepsilon_2 &= \text{measured voltage/sensitivity}_2 \\
 &= 38.87/9.56 \\
 &= 4.067\mu\varepsilon
 \end{aligned}$$

and,

$$\begin{aligned}
 E &= \sigma_2/\varepsilon_2 \\
 \sigma_2 &= E\varepsilon_2 \\
 &= 7 \times 10^4 MPa 4.067 \times 10^{-6} \\
 &= 0.2847 MPa
 \end{aligned}$$

To find the Force from this stress,

$$\begin{aligned}F_{A2} &= \sigma_1 \times Area \\ &= 0.2847 \times 64.00 \\ &= 18.22N\end{aligned}$$

The forces found, were: 18.22N and 20.57N. These should be the same, so an average value will be used.

$$F_A = 19.4N$$

Appendix D

Source Code

This Appendix contains two matlab scripts

- *Loadwavestar2.mat*: Used to transform text file from Wavestar to a matrix for analysis in matlab.
- *smo.mat*: Used to smooth the raw data that was obtained from the test run.

D.1 Loadwavestar2

This script was written by David Buttsworth.

It allows the data from the oscilloscope that has been saved as a text file by wavestar to be used in matlab

Inputs: File name, number of rows in text file and number of columns in text file.

Output: Saves the data in a matrix that can be graphed in matlab.

```
function data=load_wavestar_2(file_name,nrows,ncolumns);
fid=fopen(file_name);
fscanf(fid,'%s',ncolumns)
for i=1:nrows,
    for j=1:ncolumns,
        num1=fscanf(fid,'%f',1);
        char1=fscanf(fid,'%s',1);
        if char1=='m',
            data(i,j)=num1*1e-3;
            fscanf(fid,'%s',1);
        elseif char1=='u',
            data(i,j)=num1*1e-6;
            fscanf(fid,'%s',1);
        elseif char1=='n',
            data(i,j)=num1*1e-9;
            fscanf(fid,'%s',1);
        else
            data(i,j)=num1;
        end
    end
end
st=fclose(fid);
```

D.2 smo

This script was written by Dr David Buttsworth.

This is a moving average filter. At each data point, the data is smoothed over N points forwards and backwards of that point.

Inputs: Data series and the number of smoothing points (N)

Outputs: Smoothed data series

```
function new=smo(old,N);
%
% new=smo(old,N);
% Moving average filter. At each point in the
% series, the data is smoothed over N points
% forwards and backwards of the that point.
%
% David Buttsworth
% October 2002

len=length(old); new=old; for i=1:N,
    new(1:len-i)=new(1:len-i)+old(1+i:len);
    new(i+1:len)=new(i+1:len)+old(1:len-i);
end; new=new/(2*N+1);
```